**CIVIL ENGINEERING SERIES**
**Hydraulic Engineering Series No. # 68**

**UILU-ENG-01-2001**

**ISSN: 0442-1744**

# THREE-DIMENSIONAL HYDRODYNAMIC MODELING OF DENSITY CURRENTS IN THE CHICAGO RIVER, ILLINOIS

**By**

**Fabián A. Bombardelli[1]**

**and**

**Marcelo H. García[2]**

**[1]Research Assistant**
**[2]Professor and Director**

**Sponsored by**
**METROPOLITAN WATER RECLAMATION DISTRICT OF GREATER CHICAGO**

**VEN TE CHOW HYDROSYSTEMS LABORATORY**
**DEPARTMENT OF CIVIL AND ENVIRONMENTAL ENGINEERING**
**UNIVERSITY OF ILLINOIS AT URBAAN-CHAMPAIGN**
**URBANA, ILLINOIS**

**February 2001**

## ABSTRACT

The potential development of density currents in the Chicago River has been analyzed with the help of a three-dimensional hydrodynamic model. It was found that during the winter months, density currents can develop at the junction of the Chicago River with its North and South Branches. Such density underflows show a clear tendency to flow from the junction towards Lake Michigan. Through this subtle phenomenon, density currents are able to transport water of lesser quality along the bottom towards Lake Michigan. This phenomenon clearly explains the observations of bi-directional flow conditions made by the U.S. Geological Survey at Columbus Drive and other cross sections in the Chicago River. While this study shows that density current activity in the Chicago River is very likely, the frequency, duration, and flow discharges associated with this phenomenon have yet to be determined. Recommendations are made for more computational efforts like the current one as well as for more detailed field measurements of a number of flow and water quality parameters. A better understanding of the hydrodynamic behavior of the Chicago River over a wide range of conditions, will facilitate the management of the river system as well as the operation of the flow diversion gates and the recently constructed pumping station by Lake Michigan.

## ACKNOWLEDGEMENTS

The authors of the present report would like to thank the dataset of measurements kindly provided by the staff of the United States Geological Survey (USGS) and acknowledge their continuous help and support. Without their fundamental contribution, this project would not possible. In particular, Mr. Robert Holmes Jr., supported logistically the involvement of the University of Illinois in this project; Mr. Jim Dunker and Mr. Kevin Oberg obtained the aforementioned excellent set of measurements and Dr. Juan A. González-Castro collaborated in the preliminary analysis of the data. To all of them we are very grateful.

At the same time, the authors are very thankful for the financial support provided by the Metropolitan Water Reclamation District of Greater Chicago (MWRDGC) through a research grant (). Discussions, held at several meetings with Mr. Richard Lanyon, Mr. Irwin Polls, Mr. Bernard Sawyer and Dr. Prakasam Tata, were especially useful.

Thanks are also due to Mr. Thomas Fogarty, Chicago District US Army Corps of Engineers, for several enlightening discussions about the Chicago River at Lake Michigan.

Last but not least, this project benefited greatly from the skills of Mr. José Guzmán to render a very complicated bathymetry into a useful computational form, and the help of Mariano Cantero with the equations of state needed to assess density differences in the Chicago River. Their help is gratefully acknowledged.

# TABLE OF CONTENTS

## INTRODUCTION

Water quality in urban rivers is an issue of increasing importance at the beginning of the new millennium. Problems such as pollution due to solid urban wastes, discharges of heated water from cooling systems and contamination generated by industrial liquid effluents are quite often reported in the media and discussed in the specialized literature. Despite the existing need for more research about special aspects in environmental hydraulics of urban areas, the hydraulic engineer can currently model and measure flow discharge in urban rivers with accurate techniques.

At the same time, several previously "unforeseen" problems have appeared during the last few years, which have an important impact on the management and operation of river systems. The Chicago River (CR) has recently experienced some interesting phenomena. Very recent measurements performed by the Illinois District of the United States Geological Survey (USGS) have revealed a bi-directional flow in the river during wintertime, a phenomenon not commonly reported in the leading literature of hydraulic engineering and water quality assessment.

Motivated by this finding, the Metropolitan Water Reclamation District of Greater Chicago (MWRDGC), which manages the water flow and quality of the river, contacted researchers at the Ven Te Chow Hydrosystems Laboratory (VTCHL) at the University of Illinois at Urbana-Champaign to elucidate the causes and science of this phenomenon. Motivated by this request, the staff of the VTCHL submitted an explanation for the existence of bi-directional flow through the potential occurrence of density currents in the CR. Density currents are well known to be capable of transporting contaminants, dissolved substances, and suspended particles for very long distances. If this is the case in the CR, there could be a potential water-quality problem due to the potential for adverse impact on Lake Michigan. Further, the CR is designated to be a higher use classification by the Illinois Pollution Control Board than the North and South Branches and density currents from these adjoining water bodies could adversely impact the water quality of the CR.

The VTCHL was later asked to conduct a series of numerical experiments in order to assess the potential presence of density currents in the CR and to recommend the best locations and most appropriate techniques for performing additional measurements of the phenomenon.

This report is aimed at describing the accomplishments that have been made to date. The first Chapter deals with the description of the problem; Chapter 2 analyzes the observations made by the USGS and the MWRDGC. The third Chapter describes the theoretical model proposed for the development of density currents and Chapter 4 presents the numerical model and the computations undertaken, together with the analysis of the results. Finally, in Chapter 5, the conclusions of this study and the recommendations made for future work are presented.

# CHAPTER 1
# PROBLEM DESCRIPTION
# OBJECTIVE AND OUTLINE OF THE ANALYSIS

## 1.1 PROBLEM DESCRIPTION

By the end of the XVIII and the beginning of the XIX centuries, the CR used to flow into Lake Michigan. The littoral transport of sand at the shoreline used to block the river outfall into Lake Michigan at that time, only to be re-opened by flooding events in the CR. An interesting compilation of the historical evolution of the river mouth can be found in Chrzastowski (1998).

During the latter part of the XIX century, a continuing public health problem existed because untreated wastewater from Chicago was carried by the CR into Lake Michigan, the source of Chicago's public water supply. This problem, which caused the death of thousands of inhabitants, motivated the artificial modification of the direction of flow in the river, which, since 1900, goes from the lake towards the West (Figure 1.1). This change, accomplished through the construction of a 28-mile canal and 12 miles of river improvements during the 1890s, and the installation of gates and a diversion system at the shoreline during the 1930s, constitutes one of the major river engineering achievements of the last century (see Lanyon, 2000).

The flow from the lake to the CR is not continuous. During the summer months (more precisely, from June through October), water is diverted from the lake to the river by the MWRDGC, in order to preserve its water quality. Two other different sources contribute to the flow in the CR, as follows:

a) The inflow resulting from locking (passage of boats and ships from the lake to the CR and viceversa), mainly during summertime and

b) the uncontrolled leakage through aging gates and walls.

The amount of leakage and locking inflow depends on the water level difference between Lake Michigan and the CR. The United States Army Corps of Engineers (USACE) initiated a set of reparation activities on the lock gates in late 1997 that lasted till early 1999. The Illinois Department of Natural Resources (IDNR) constructed new walls in 1999 and 2000. Therefore, the amount of water entering the river through leakage is supposed to be minimum nowadays.

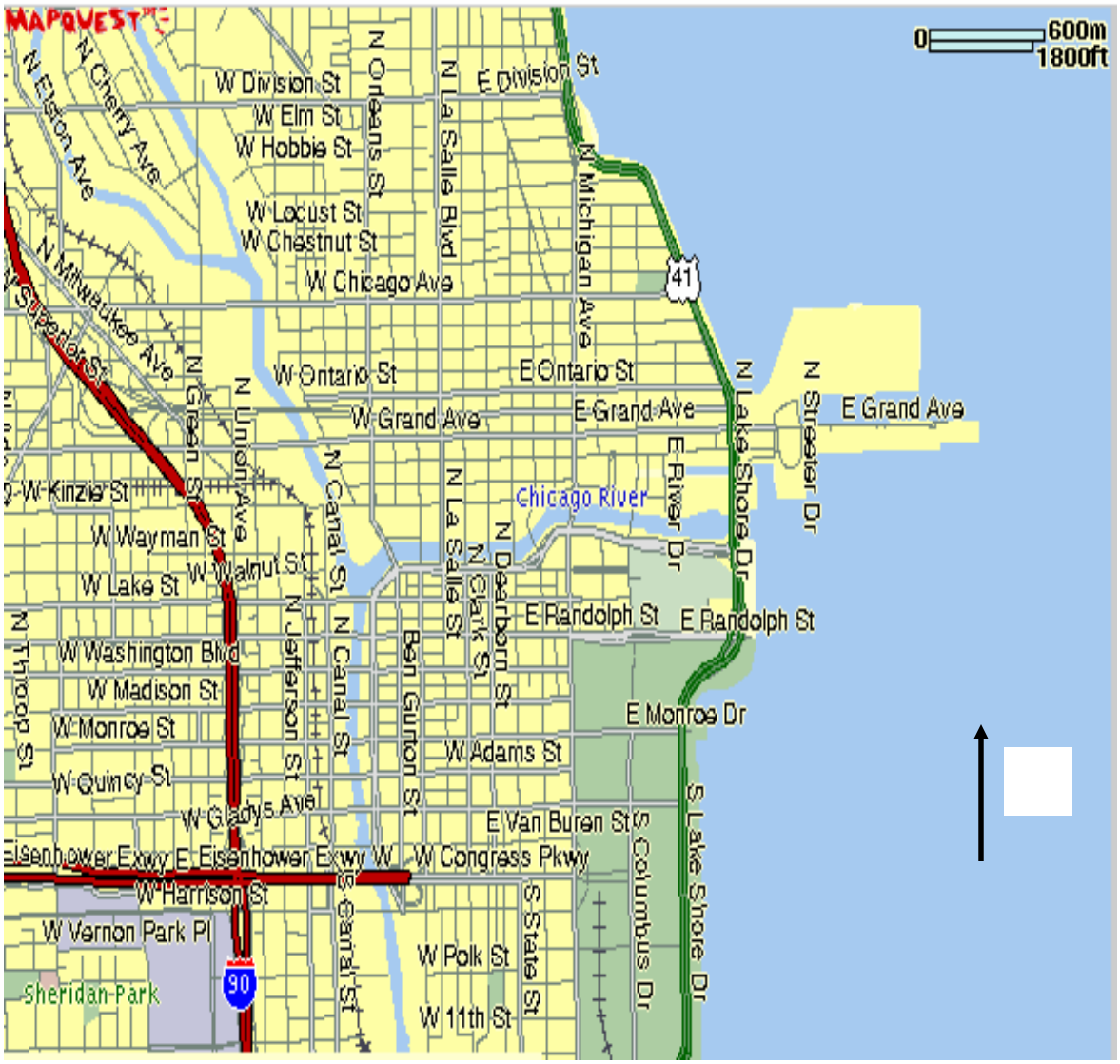


**Figure 1.1:** Map of the zone of interest in downtown Chicago

The waters of the CR merge with the flow coming from the North Branch of the Chicago River (NBCR), forming the South Branch of the Chicago River (SBCR); see Figure 1.1. The NBCR carries treated municipal sewage effluent released by a plant located several miles upstream of the confluence of the branches; the discharge of the effluent is about 280 MGD, which is equivalent to 12.3 $m^3/s$.

The system of channels locally receives waters from direct precipitation and discharges from neighboring areas. Particularly, some of the buildings located in the riverbanks (Figure 1.2) use water for cooling purposes and, in doing so, can potentially have an effect on water quality.


**Figure 1.2:** Aerial view of the mouth of the CR from Lake Michigan

In November 1999, the IDNR Department of Water Resources, based on an aerial photograph, reported a noticeable difference in the color of the water between Lake Michigan and the CR, which was later confirmed by the MWRDGC. Since common sense suggests that darker water could be of poorer quality, the MWRDGC decided to collect samples in the CR for water-quality analysis. Measurements taken by the USGS a year earlier as well as new ones were gathered to analyze the possible causes of the phenomenon. The observations obtained by the USGS revealed the presence of a bi-directional flow. Velocities were observed going towards the lake along the bottom and towards the junction along the upper layer of the water column. These observations have motivated the research presented herein.

## 1.2 DENSITY CURRENTS

Density currents are flows driven by density differences. In the field, they may be initiated by diverse mechanisms, such as the direct inflow of turbid river water, subaqueous slumps induced by seismic or other disturbances, artificial discharge of mining tailings, temperature gradients or dredging operations (García, 1994). It is possible to distinguish between two types of turbidity currents: discontinuous or surge-like currents and the continuous or plume-like currents. Discontinuous currents are usually generated by instantaneous sources of suspended sediment and they are consequently events of limited duration. For example, earthquakes and dredging operations can trigger discontinuous turbidity currents. Continuous currents, on the other hand, can last for hours and even for days (García, 1992; García, 1994).

Figure 1.3 shows a density current observed in the laboratory (García, 1990), in which the visualization has been enhanced by the addition of fluorescein. It is possible to notice the typical shape of the front where a substantial amount of mixing takes place.

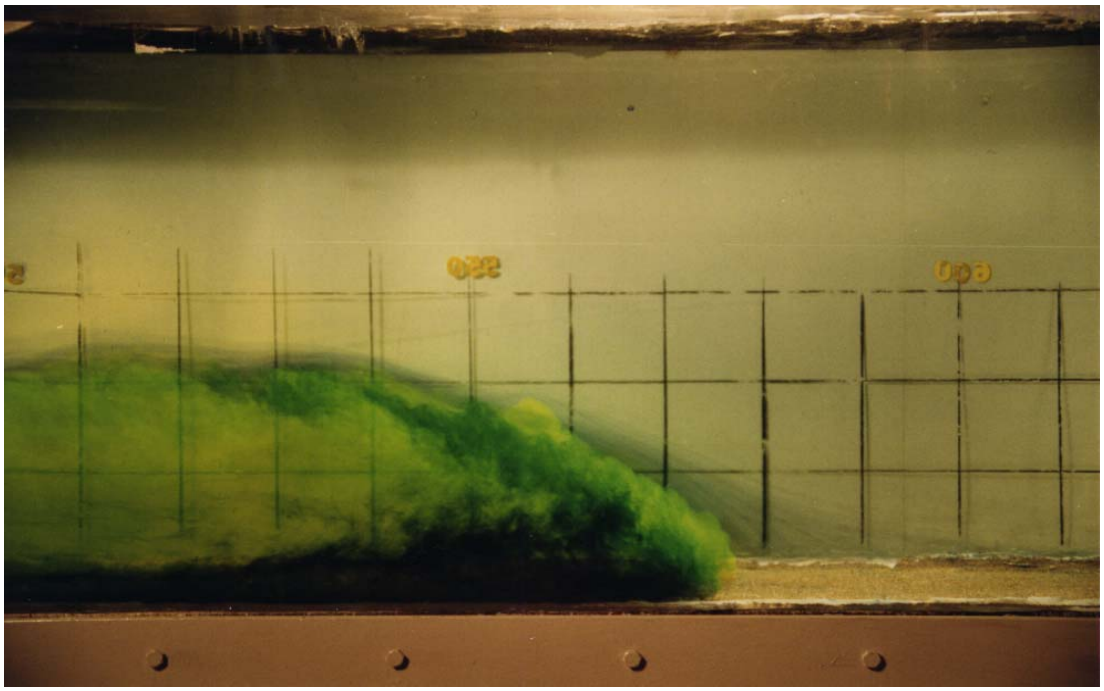

**Figure 1.3:** Density current obtained in the laboratory (García, 1990)

## 1.3 OBJECTIVES OF THIS WORK

The objectives of the computational effort reported herein are as follows:

a) to assess the potential development of density currents in the CR and the conditions when such phenomenon could take place, and
b) to recommend the best locations and most appropriate techniques for conducting observations of the phenomenon.

## 1.4 OUTLINE OF THE ANALYSIS

The analysis carried out at this stage of the project comprises the following steps, which are described in the foregoing chapters:

1) Understanding of the problem, including the analysis of previous measurements;

2) formulation of a theoretical model;
3) numerical solution of the theoretical model;
    a. analysis of the problem in an idealized domain;
    b. analysis of the problem within the real bathymetry.

The approach proposed for the solution of the problem is based on the concept of enhancing the understanding of the phenomenon through field observations. Only from a sound understanding of the phenomenon, a satisfactory theoretical model can be built and correct questions can be posed. At the same time, it is clear that a thorough understanding of the physics involved in the phenomenon would be very valuable in helping with the operation of the system.

It is also important to point out that more measurements are still needed to validate the theoretical and numerical models presented herein. Several aspects of the phenomenon still need to be clarified and more observations, some of them being currently undertaken, will most likely shed light on the frequency of occurrence of this kind of density-driven underflow.

# CHAPTER 2
# ANALYSIS OF THE OBSERVATIONS OBTAINED BY THE USGS AND MWRDGC

The information analyzed in this chapter is based on observations made by the USGS (personal communication) and a report generated by the MWRDGC (Polls et al., 2000). It refers to measurements of flow velocity, water temperature, specific conductance, dissolved oxygen (DO), suspended solids, turbidity, ammonia, nitrates, nitrogen and total phosphorus.

## 2.1 MEASUREMENTS OF FLOW VELOCITY

The USGS has placed a permanent Acoustic Velocity Meter (AVM) at the bridge crossing over the CR on Columbus Drive. This device converts backscattered acoustic pulses into electrical signals that are recorded digitally. Figure 2.1 presents a schematization of the features of the installation of the AVM at Columbus Drive, provided by the USGS.

The AVM was able to detect a bi-directional flow on January 11, 1998 (see Figure 2.2b), but a unidirectional profile on January 6, 1998 (see Figure 2.2a). The positive sign in those plots indicates flow from East to West. Thus, in Figure 2.2b, the lower part of the velocities points to Lake Michigan (negative values). The small plots on top of each figure depict the turbulent signal for the streamwise component of velocity in the CR, as recorded by the AVM; a vertical line indicates the instant at which the vertical velocity profile was measured. *It is possible to see that in Figure 2.2a, the existing conditions were those of an important flow discharge in the CR towards the junction between the NBCR and the SBCR. On the other hand, in Figure 2.2b, the flow velocities were quite small. This result would suggest that bi-directional flows are concomitant with close-to-null flow discharge in the CR*.

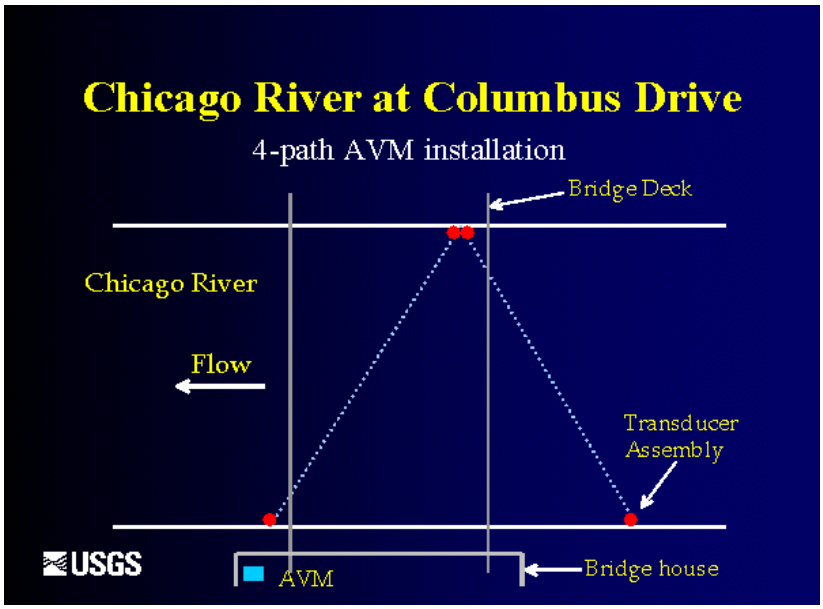


**Figure 2.1:** Schematic of the AVM installation

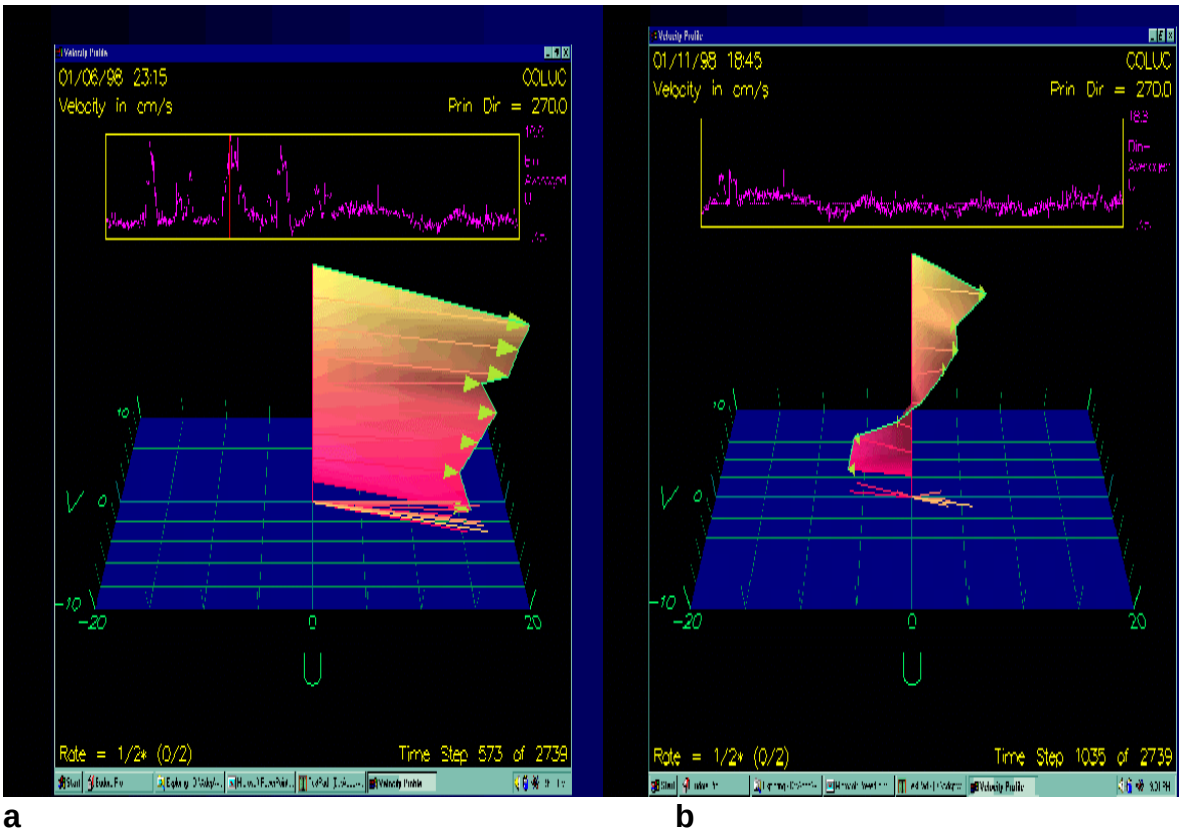


**a** **b**

**Figure 2.2:** Velocity measurements at Columbus Drive

Both Figures 2.2 give an idea of the intensity of the velocities involved: whereas the flow velocity on January 6 reached values as large as 0.2 m/s (20 cm/s=0.66 ft/s), the maximum streamwise velocities during January 11 were + 0.06 m/s (0.197 ft/s) and –0.07 m/s (-0.23 ft/s). Additionally, it is possible to note that the vertical point with zero velocity (i.e. where the flow changes direction) is located at about 0.33 of the flow depth, that is 2.3 m (7.6 ft) from the bottom.

Figure 2.3 presents a two-dimensional view of the velocity measurements at the Columbus Drive cross section on February 19, 1998. The velocities are plotted with the aforementioned sign convention. The velocity vectors in fact point perpendicularly to the paper. It is possible to clearly notice the bi-directional flow, i.e., the same flow pattern observed one and a half months earlier during 1998. It is also noteworthy that the distribution of velocities within the vertical is similar throughout the whole cross section; that is, the vertical profile showed in Figure 2.2b repeats itself across the whole width. Again, the maximum positive and negative velocities are comparable in magnitude and similar to those shown in Figures 2.2: 0.2 ft/s. Also, the location of the height of zero velocity is at about 45 % of the flow depth above the bottom.

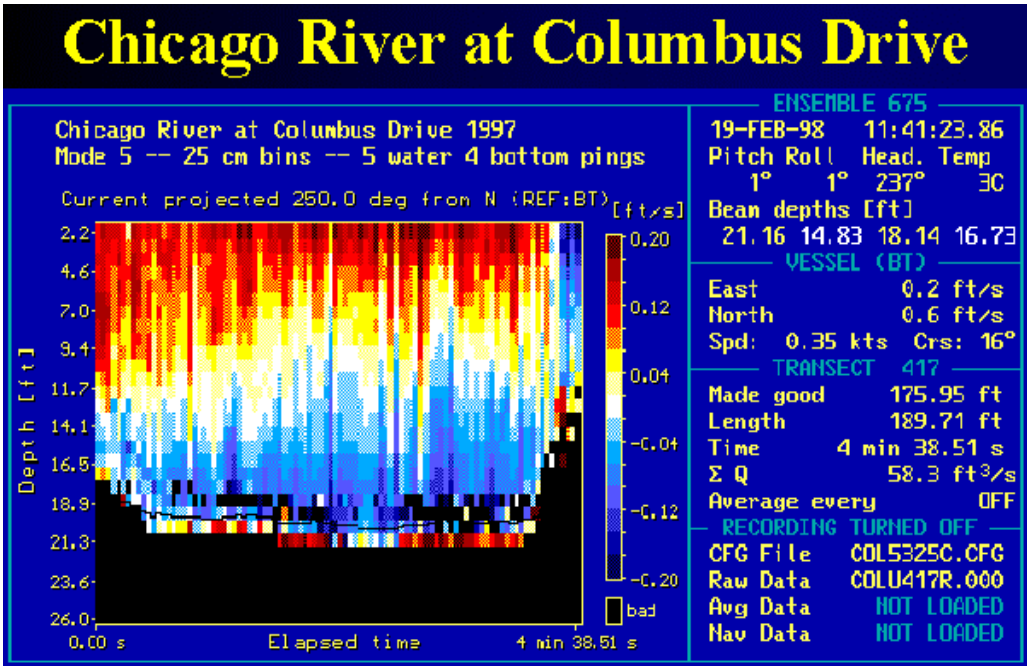


**Figure 2.3:** Velocity measurements at Columbus Drive (02/19/98)

Figure 2.4a shows more vertical profiles of streamwise velocity, taken in March, 1998, one month later than the measurements presented above, at different cross sections along the CR: McClurg Court, Wabash Avenue, La Salle Street and, again, Columbus Drive. These measurements were obtained with an Acoustic Doppler Velocimeter (ADV) with the exception of Columbus Drive, in which and ADCP was used. It is seen that the flow pattern is the same, with velocities pointing to Lake Michigan right above the bottom. Most of the profiles show maximum velocities of about -0.10 ft/s and +0.15 ft/s, in concomitance with the above results. The positions of the height of zero velocity oscillate in the figures, as follows: 0.74 of the flow depth in McClurg Court, 0.58 in Wabash Avenue, 0.55 in La Salle Street and 0.5 in Columbus Drive. Figure 2.4b is a comparison of the vertical velocity profiles across the cross section; it is noticed that the profiles are relatively similar, which agrees well with Figure 2.3.

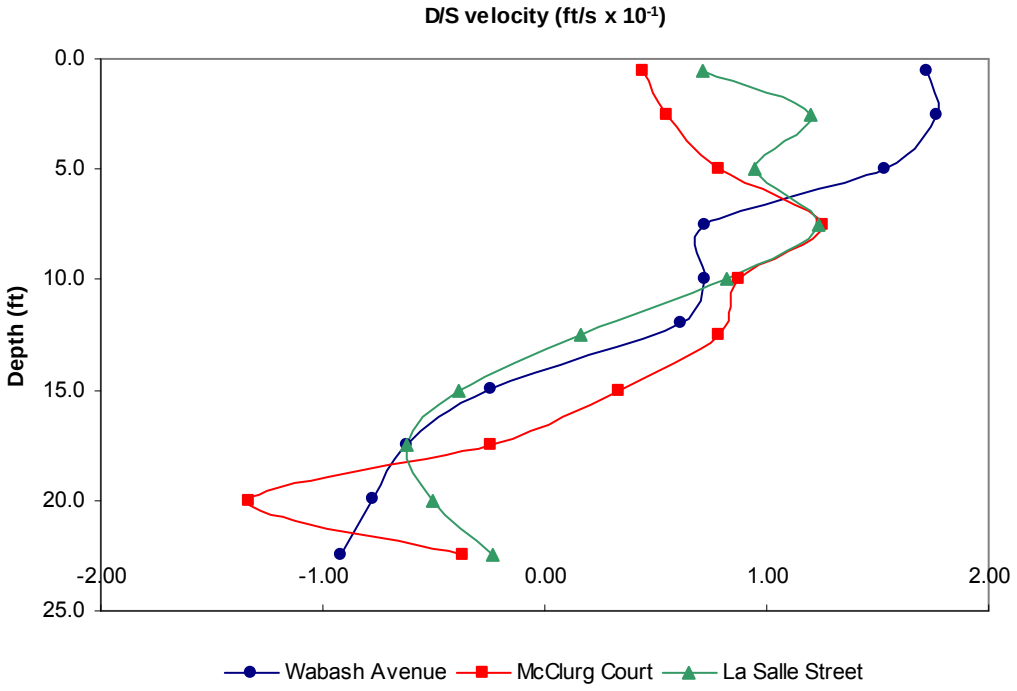


**Figure 2.4a:** Velocity measurements at three different cross sections (03/18/98)

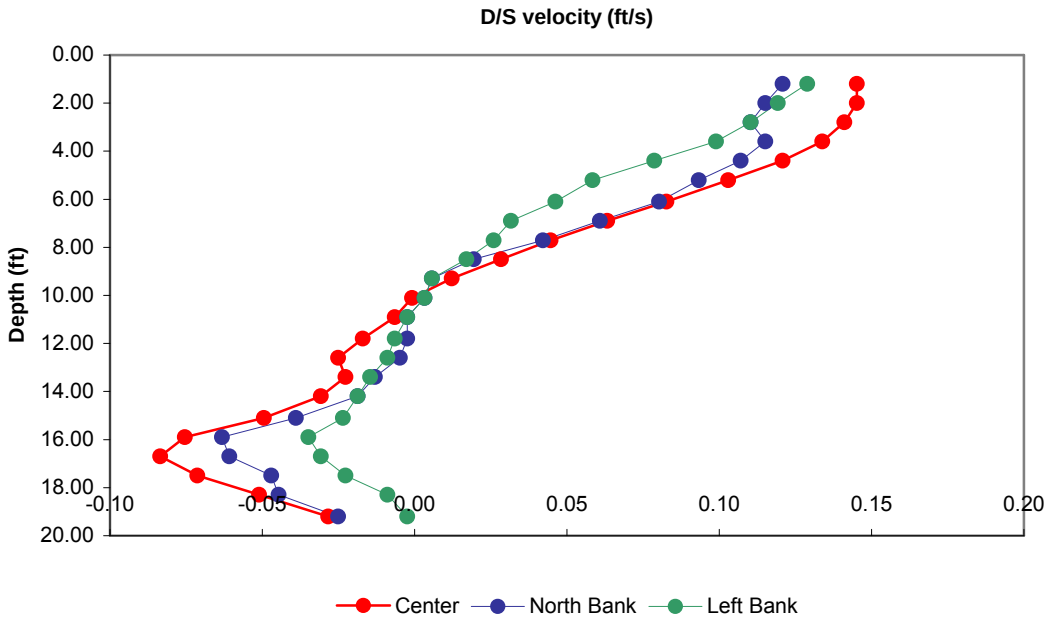


**Figure 2.4b:** Velocity measurements at Columbus Drive (03/18/98)

Interestingly, these bi-directional flows were not detected by USGS measurements during summertime, when the flow towards the junction is relatively intense (one should recall the contribution from locking activities as it was mentioned in Chapter 1). Therefore, *the simultaneous presence of low flows in the CR and bi-directional vertical profiles is once again observed, reinforcing the idea that bi-directional flows occur mainly when there is no mean flow discharge in the CR*.

These types of flow velocity distributions could be attributed "a priori" to wind-induced flows or to density currents. This issue will be analyzed later.

## 2.2 MEASUREMENTS OF WATER TEMPERATURE AND CONDUCTIVITY

The USGS conducted observations of water temperature and electrical conductivity in various cross sections of the CR in March 18 and 19, 1998 and of temperature only on February 24, 1998. Figures 2.5a-g present the distributions of temperature in several locations (Lake Shore Drive, Columbus Drive, Michigan Avenue,

Wabash Avenue, State Street and Franklin/Orleans Street), while Figures 2.6a to f depict the distributions of specific conductance in those locations; Tables 2.1a-g detail the measured values, expressed in degrees centigrade for temperature and in microsiemens per centimeter (µS/cm) for conductance. This last variable is a surrogate for the content of total dissolved solids (TDS) and is a measure of the ability of a solution to transmit an electrical current. It depends on the total concentration of ionized substances dissolved in water and the values are expressed at 20 or 25 °C. For the measurement of these variables, multi-parameter, water-quality-monitoring instruments, manufactured by Hydrolab Corporation, Austin, Texas, were employed, with an accuracy of +/- 0.15 °C for temperature and +/- 1 % in range for conductivity (range: 0 to 100 µS/cm).

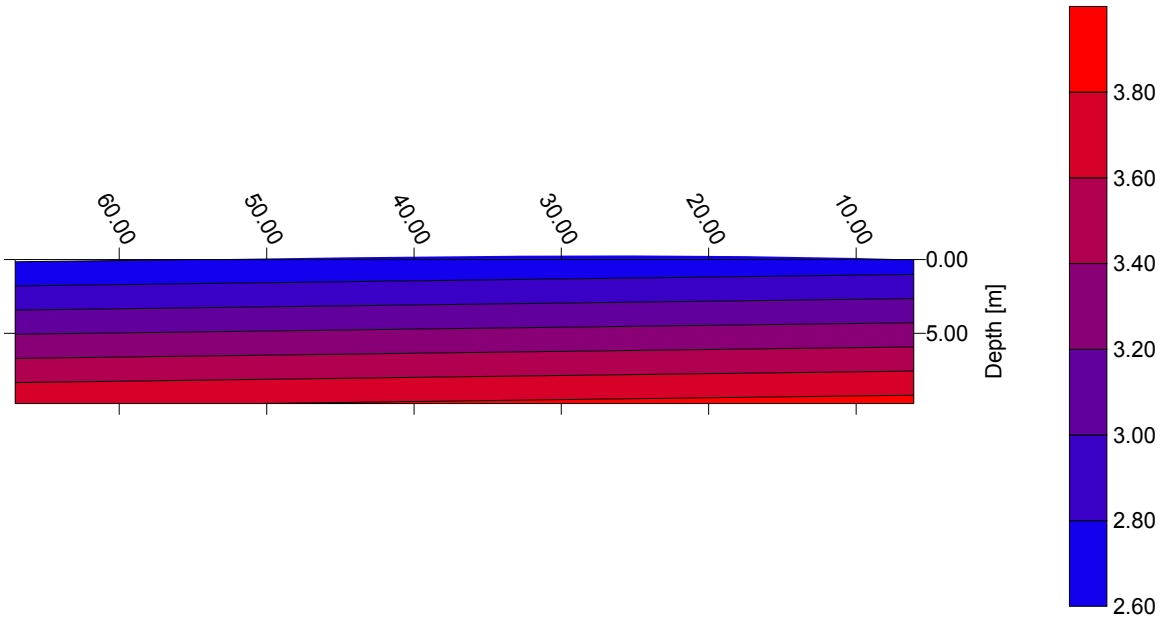


**Figure 2.5a:** Temperature distribution at Lake Shore Drive (03/19/98)

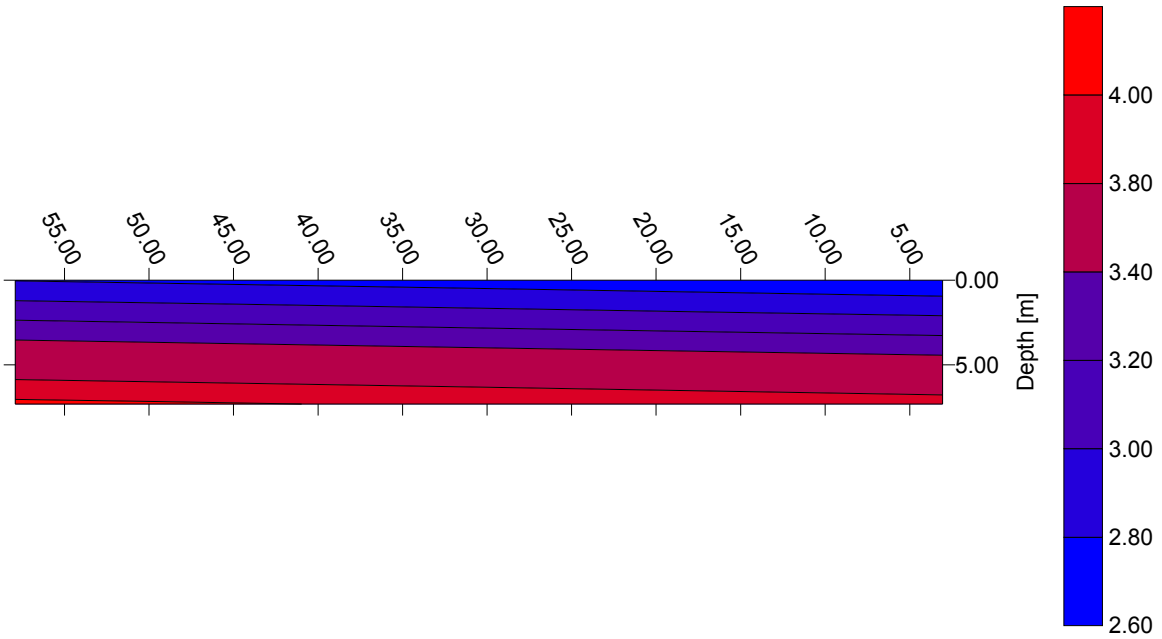


**Figure 2.5b:** Temperature distribution at Columbus Drive (03/19/98)

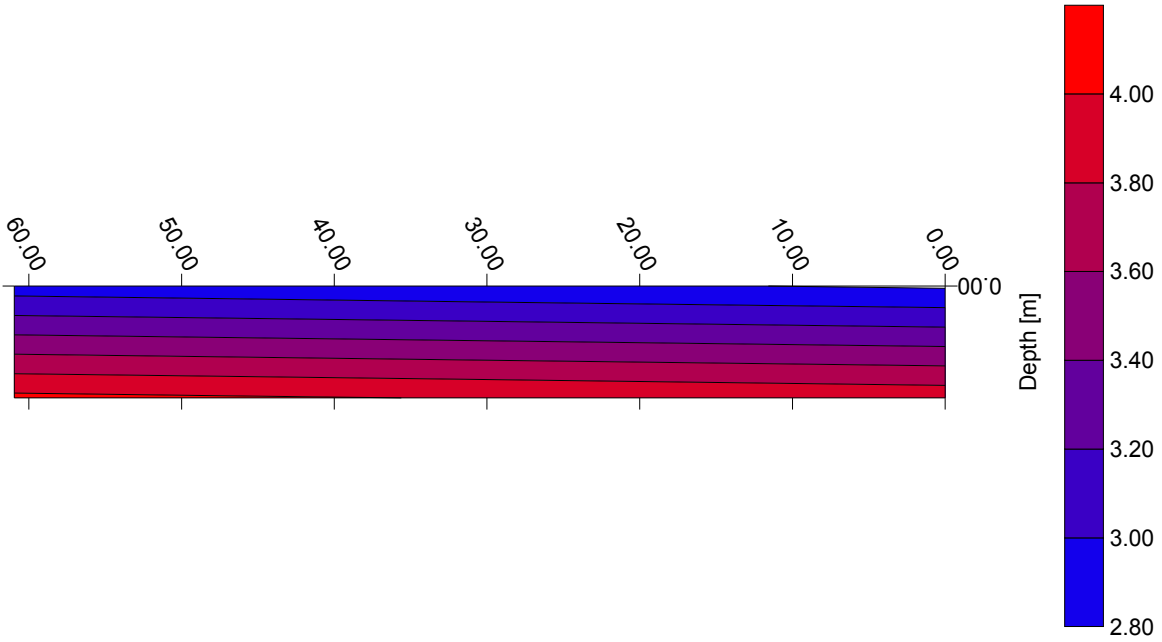


**Figure 2.5c:** Temperature distribution at Michigan Avenue (03/19/98)

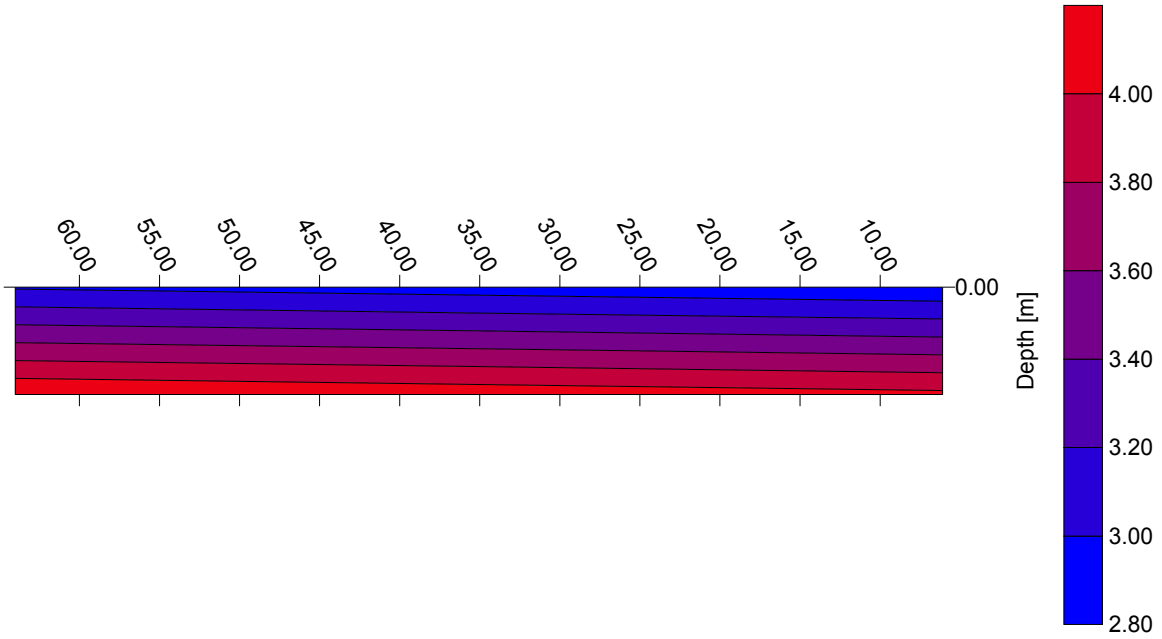


**Figure 2.5d:** Temperature distribution at Wabash Avenue (03/19/98)

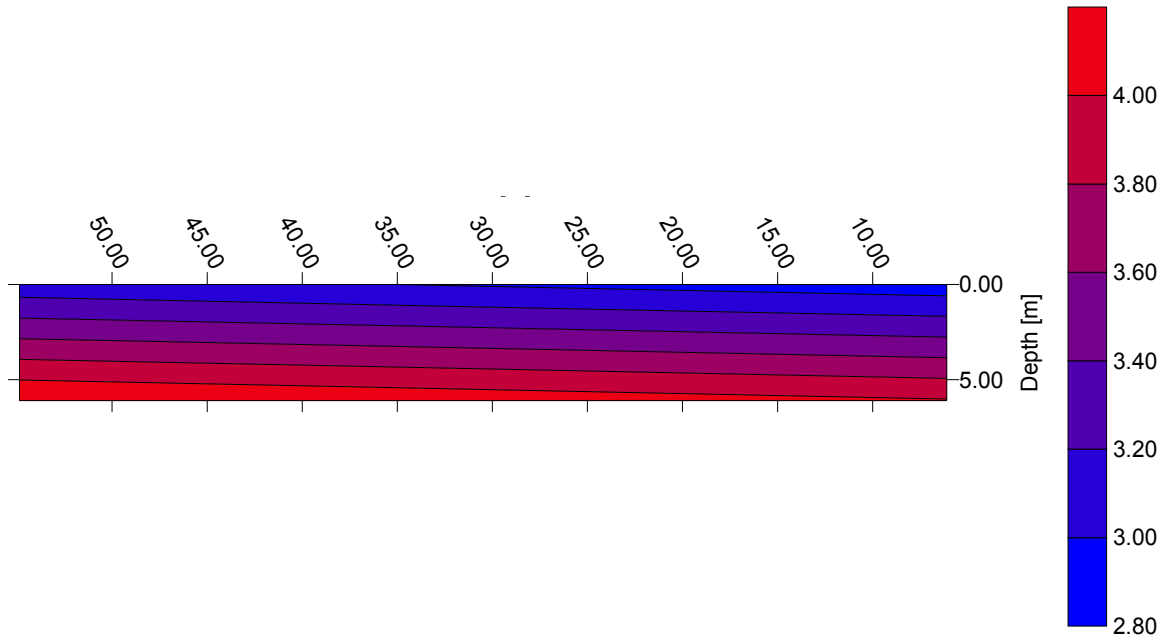


**Figure 2.5e:** Temperature distribution at State Street (03/19/98)

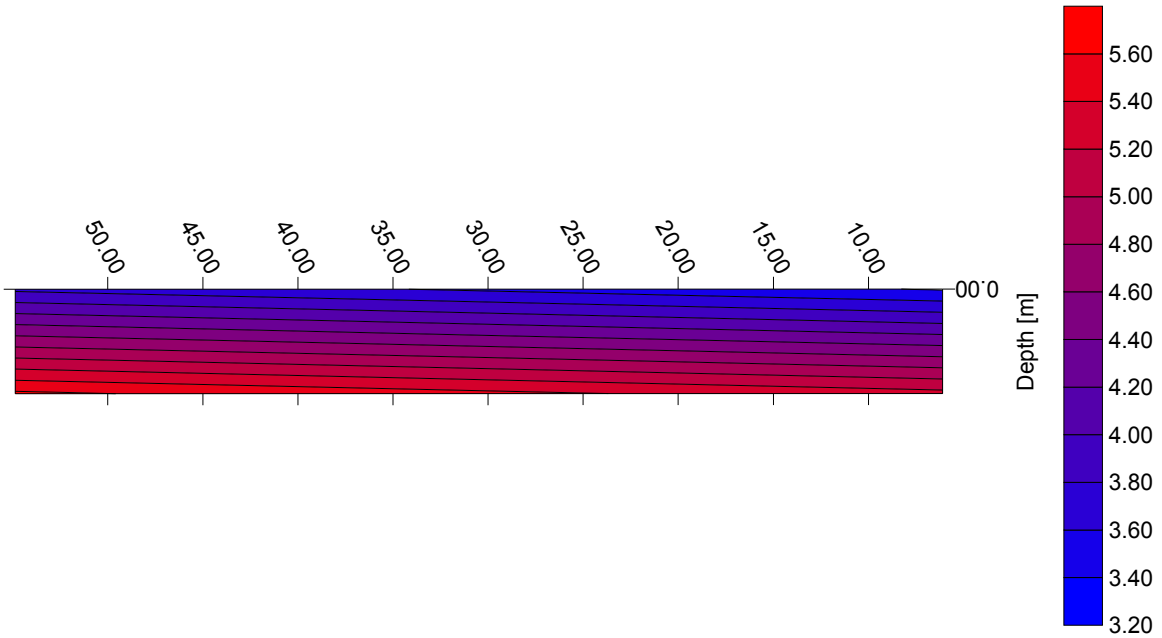


**Figure 2.5f:** Temperature distribution at Franklin/Orleans Street (03/19/98)

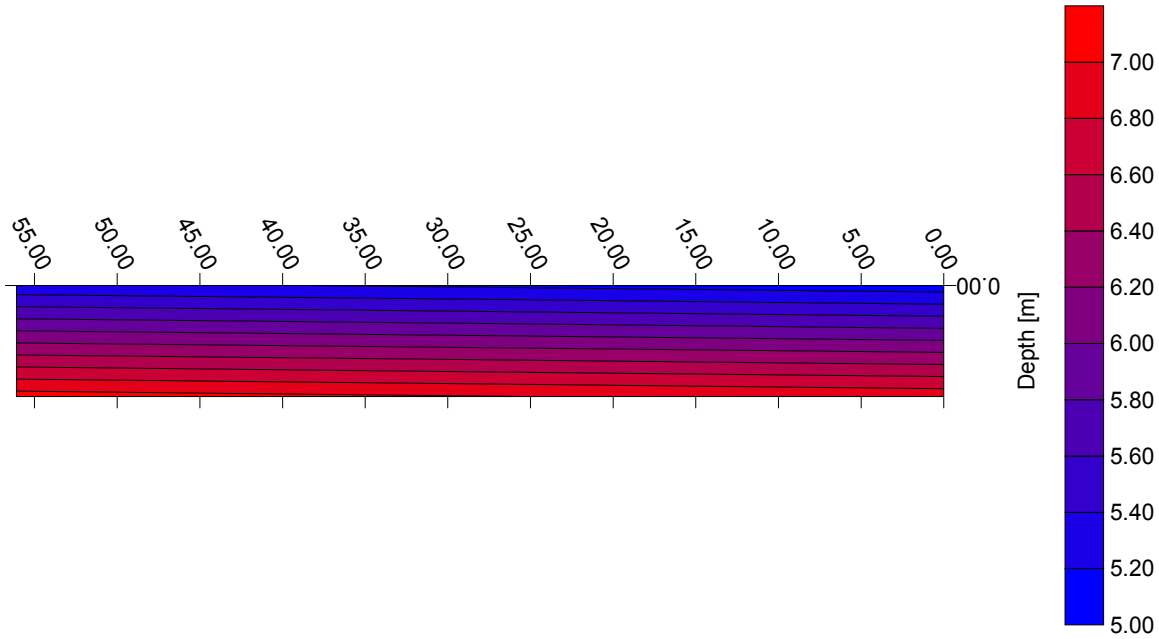


**Figure 2.5g:** Temperature distribution at Columbus Drive (02/24/98)

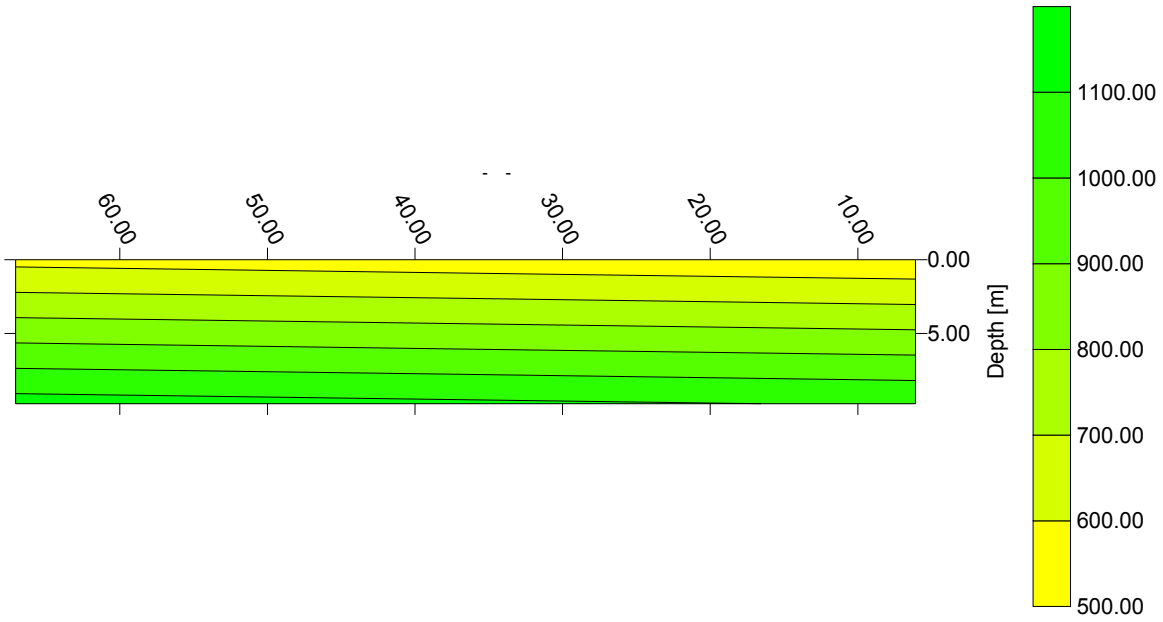


**Figure 2.6a:** Specific conductance distribution at Lake Shore Drive (03/19/98)

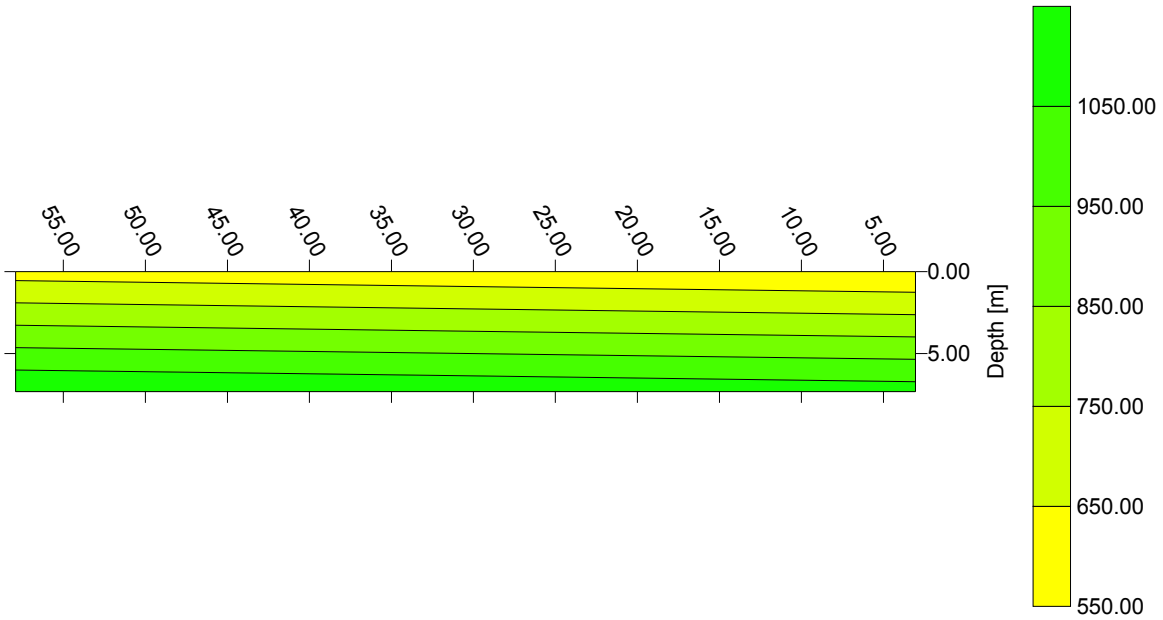


**Figure 2.6b:** Specific conductance distribution at Columbus Drive (03/19/98)

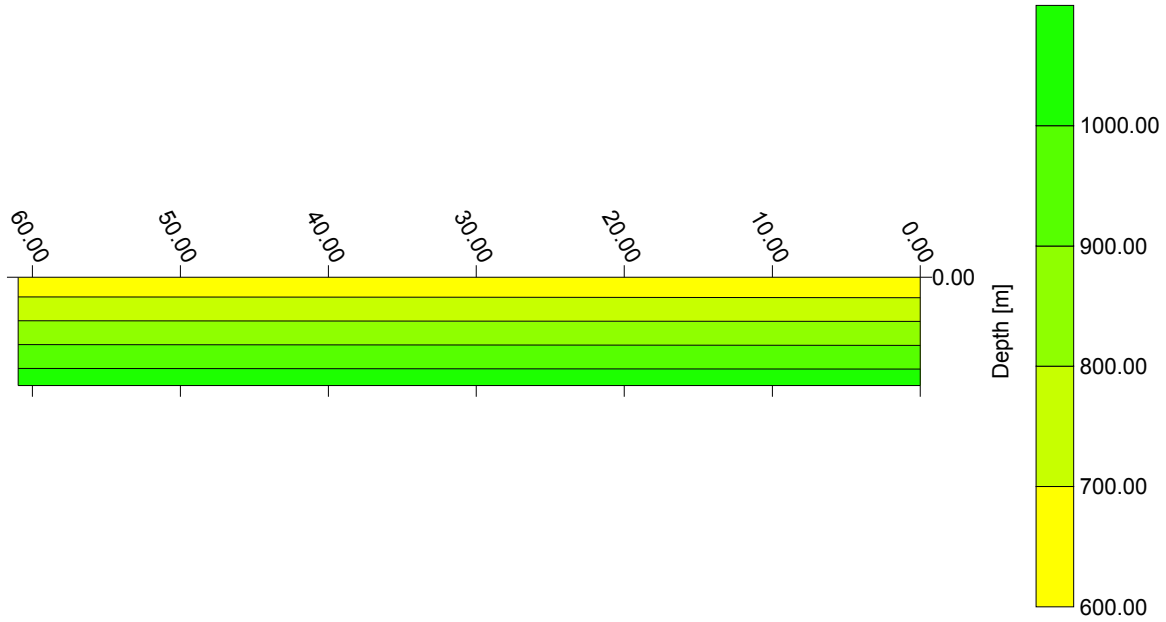


**Figure 2.6c:** Specific conductance distribution at Michigan Avenue (03/19/98)

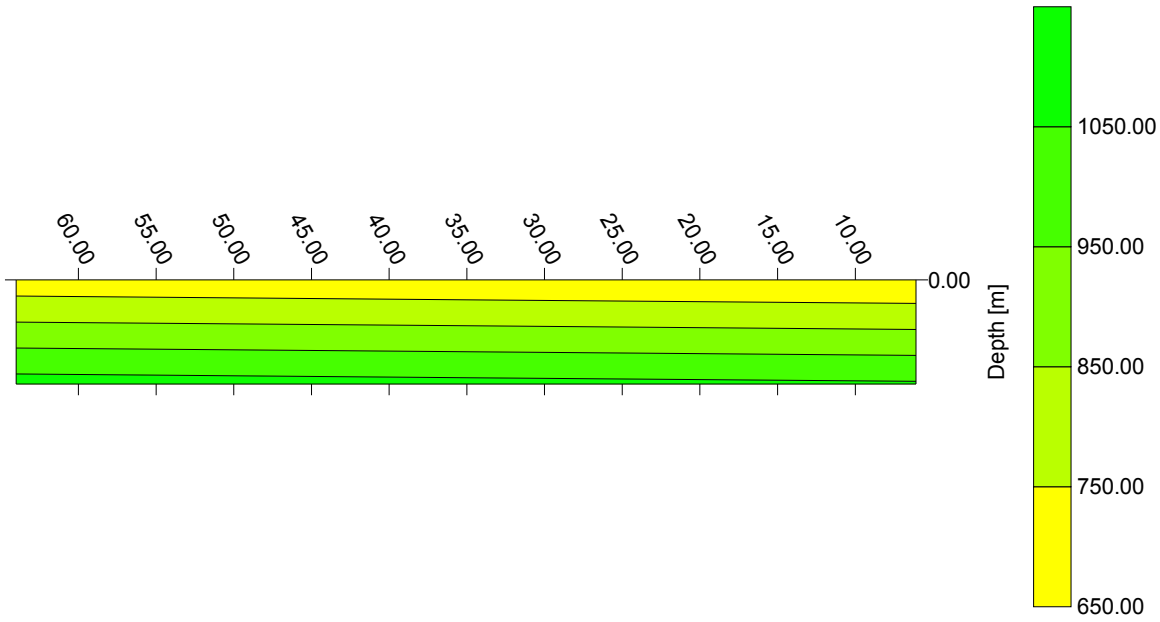


**Figure 2.6d:** Specific conductance distribution at Wabash Avenue (03/19/98)

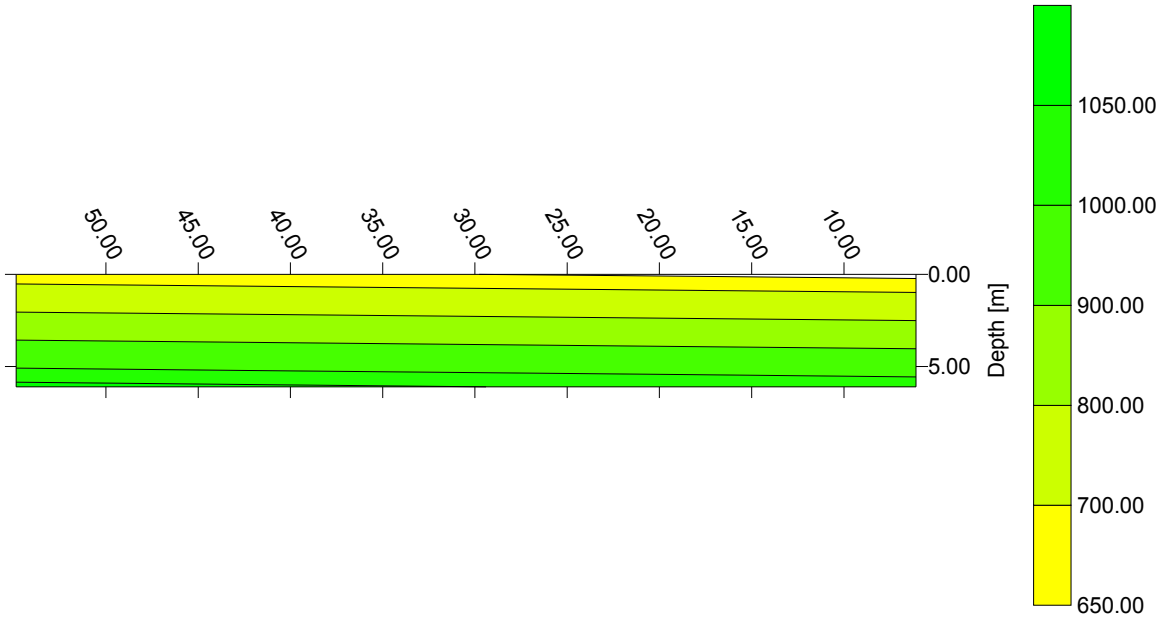


**Figure 2.6e:** Specific conductance distribution at State Street (03/19/98)

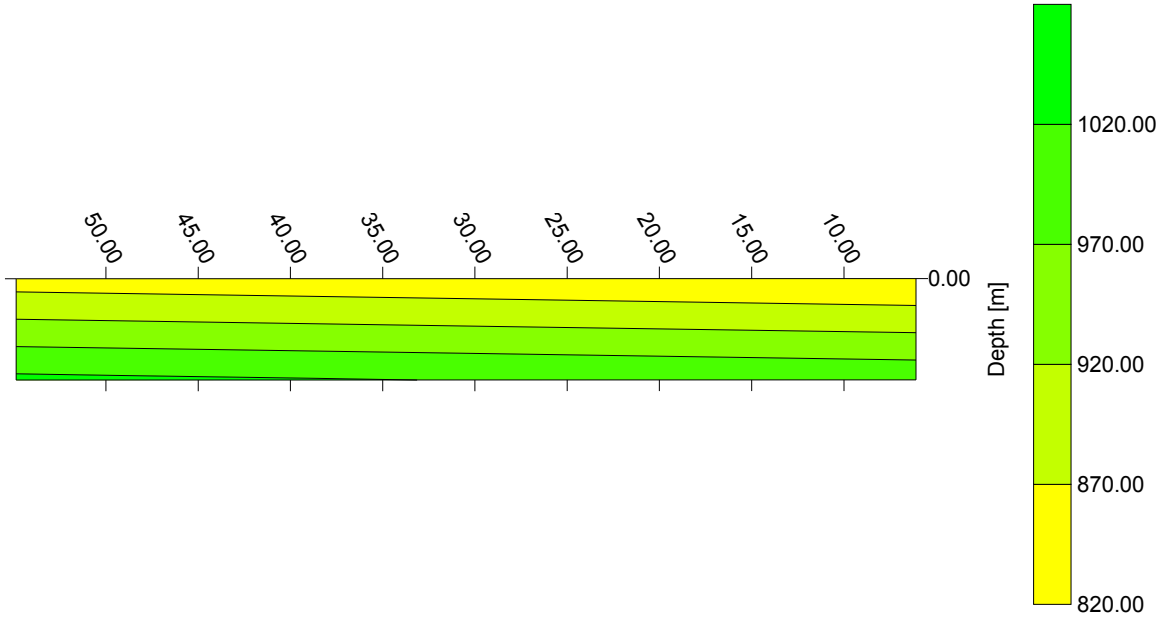


**Figure 2.6f:** Specific conductance distribution at Franklin/Orleans Street (03/19/98)

Several linear regressions have been proposed to relate the content of total dissolved solids with the conductance, but in all the equations the latter increases with the content of TDS. However, *there is no universal linear relation between TDS and conductivity (USGS, 2000)*. In general, it is commonly accepted that:

$$TDS\ (in\ mg/l) = k\ SC\ (in\ \mu S/cm) \tag{2.1}$$

where $k$ takes values from 0.5 to 0.75. From the book by Snoeyink and Jenkins (1987, page 92), a value of 0.64 can be obtained.

From previous plots, it is possible to note that larger temperatures are located in the lower part of the cross sections. Interestingly, for these observations, the temperatures in some cases pertain to stable situations (because all the temperatures within the cross sections are smaller than 4° C, the point of maximum water density, and the bigger temperatures are found along the bottom, see next points), such as in Lake Shore Drive, Columbus Drive, Michigan Avenue and Wabash Avenue, but they lead to unstable conditions in other cross sections.

For the conductance, it was assumed that all the values were corrected to the standard temperature. All the distributions show a stable pattern, consisting in larger values towards the lower part of the cross sections. Adopting the value of 0.64 for $k$, it is possible to note that concentrations of TDS up to 630 mg/l are present at different cross sections.

## 2.3 MEASUREMENTS CONDUCTED BY THE MWRDGC

The staff of MWRCGC performed a set of water-quality measurements of water temperature, dissolved oxygen (DO), suspended solids, turbidity, total ammonia nitrogen, nitrate nitrogen and total phosphorus at four stations within the CR (Clark Street, Michigan Avenue, McClurg Court and Chicago River Lock) and one station in each of the branches (Erie Street in the NBCR and Jackson Boulevard in the SBCR).

Additionally, four stations have been located in Lake Michigan (Polls et al., 2000). The observations were conducted consecutively during 5 weeks (from November 30 to December 21, 1999), one day a week (every Tuesday). The measurements correspond to one vertical per cross section, and only a single value for each cross section is provided.

The conclusions of the MWRDGC report were as follows:

a) the NBCR shows systematic higher temperatures than the CR and the SBCR; temperatures in the SBCR are also larger than the counterparts in the CR. The temperature differences among the three branches are smaller than 5 °C; Lake Michigan presents much lower temperatures than the three branches;
b) both the NBCR and SBCR present lower concentrations of DO than the CR; in the latter water course, the concentration of DO increases from the junction towards Lake Michigan;
c) suspended solids concentrations, turbidity levels and nutrients concentrations are higher in the NBCR than in the SBCR and, in the SBCR, they are larger than in the CR.

The details of all the measurements can be found in Polls et al., 2000. The main conclusion of these tests is that *the NBCR clearly shows poorer water-quality conditions than the SBCR and than the CR itself. This is also concomitant with the existence of a treatment plant upstream of the junction, which constitutes the major flow source for the NBCR*. Polls et al. suggest that water from the lake had to be flowing into the CR in order to generate the above dilution, by virtue of the date of the measurements (the discretionary diversion ceases by the beginning of November), but this interpretation could be reversed: water with poorer water quality could be entering the CR and this influence could decay within it, as indicated by the water-quality measurements.

The concentrations of suspended solids measured by MWRDGC reached values of 28 mg/l in the branches and in the CR itself.

## 2.4 PROCESSING AND ANALYSIS OF THE USGS MEASUREMENTS

The information provided by the USGS constitutes the most complete resource of data about the hydrodynamics in the CR. Analyzing the data, it was necessary to elucidate some of the features of the observations. In fact, some of the temperature measurements indicate that the water density is smaller in the lower part of the cross section (which would lead to unstable flow conditions) whereas the distribution of conductivity shows larger densities near the bottom and, thus, a stable pattern. It is well known that water density can be computed as the sum of the value corresponding to a certain temperature, plus a correction accounting for the presence of suspended solids (SS) and a second correction due to dissolved solids (DS), as follows:

$$\rho(T,\, SS,\, DS) = \rho_0(T) + \Delta\rho_{SS} + \Delta\rho_{DS} \tag{2.2}$$

Several authors have provided different expressions for excess fractional density, in terms of the contents of suspended and dissolved solids, respectively. In some cases, the temperature has been included in the corrections.

For the basic density in terms of water temperature, Gill (1982) presented the following polynomial:

$$\rho = 999.842594 + 6.793952\ 10^{-2}\ T - 9.095290\ 10^{-3}\ T^2 + 1.001685\ 10^{-4}\ T^3 +$$

$$-1.120083\ 10^{-6}\ T^4 + 6.536332\ 10^{-9}\ T^5 \tag{2.3}$$

where $T$ is the temperature given in °C and the density is measured in kg/m$^3$. Wüest et al. (1992) reproduced in turn the following polynomial:

$$\rho = 999.868 + 10^{-3}\left(65.185\ T - 8.4878\ T^2 + 0.05607\ T^3\right) \tag{2.4}$$

For the correction of dissolved solids, two alternatives can be found. The first one is to express the content of solids in the form of *total dissolved solids* (TDS); the other is to express that content in the form of *salinity* (S). In terms of the TDS, Ford and Johnson (1983) have proposed:

$$\Delta \rho_{DS} = C_{TDS} \left( 8.221\ 10^{-4} - 3.87\ 10^{-6}\ T + 4.99\ 10^{-8}\ T^2 \right) \tag{2.5}$$

where $C_{TDS}$ is the concentration of total dissolved solids in g/m$^3$ or mg/l. It can be noticed that the influence of the temperature is not so important when the range of variation of temperature is quite small. Figure 2.7 shows the ratio of $\Delta \rho_{DS} / C_{TDS}$ as a function of temperature. It is possible to conclude that a change of only 10 % occurs in that ratio when the temperature varies from 0 to 40 °C. If the change is small (say, from 2 to 6 °C), the variation of the ratio is very small.

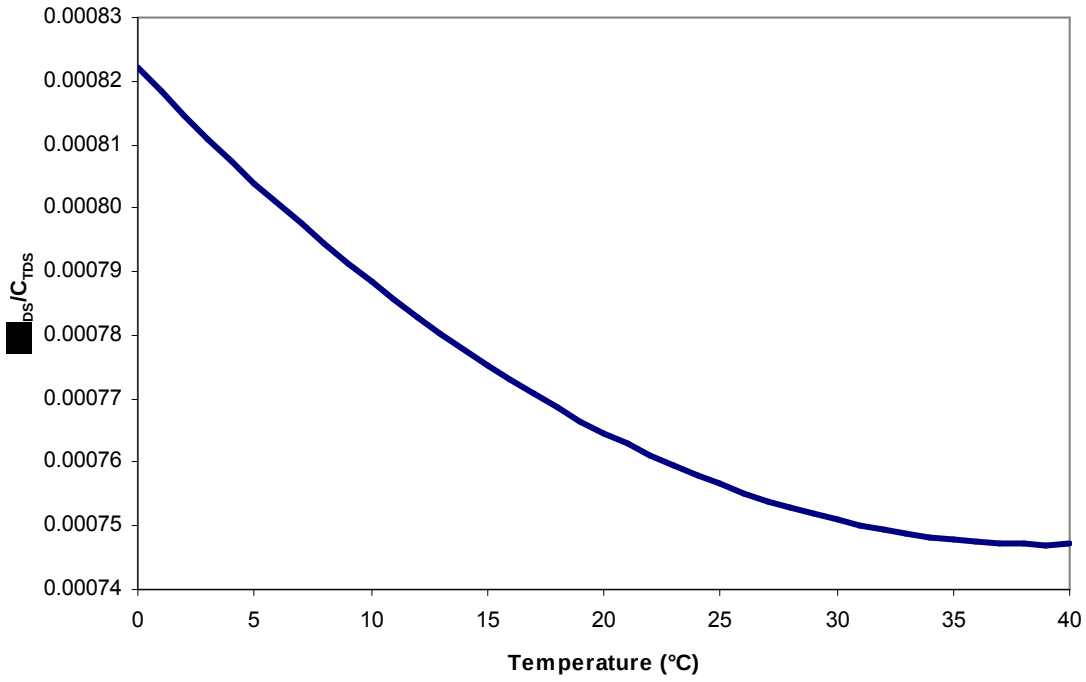


**Figure 2.7:** Plot of equation 2.5 in terms of temperature

If the content of dissolved solids is expressed in terms of salinity, Gill (1982) presents the following formula:

$$\Delta \rho_{DS} = C_{SL} \left(0.824493 - 4.0899\ 10^{-3}\ T + 7.6438\ 10^{-5}\ T^2 - 8.2467\ 10^{-7}\ T^3 + 5.3875\ 10^{-9}\ T^4\right) +$$

$$+ C_{SL}^{1.5} \left(-5.72466\,10^{-3} + 1.0277\ 10^{-4}\ T - 1.6546\ 10^{-6}\ T^2\right) + 4.8314\ 10^{-4}\ C_{SL}^2 \quad (2.6)$$

where $C_{SL}$ is the salinity expressed in kg/ m$^3$ (very often, salinity is defined as the ratio between the weight of salt and the sum of the weights of salt and water).

Wüest et al. (1992), in turn, simply added a term to Equation 2.4, as follows:

$$\Delta \rho_{DS} = \psi\ C_{DS} \quad (2.7)$$

where $\psi$ is either 0.802 kg/m$^3$/‰ if the salinity is expressed as dissolved salt content in per mil or 0.705 $10^{-3}$ kg/m$^3$/(µS/cm) if the concentration is expressed in terms of the electrical conductivity measured at 20° C.

The correction for suspended solids can be done using the following well-known relation (García, 1990):

$$\frac{\Delta \rho}{\rho} = R\ C_{SS} = \frac{(\rho_s - \rho)}{\rho}\ C_{SS} \quad (2.8)$$

where $R$ denotes the submerged specific gravity and $\rho_s$ is the density of the suspended solids.

Data reporting contents of suspended solids are not abundant. The measurements performed by MWRDGC were used to have an idea about the amount in

density change that could be attributed to them. Applying Equation 2.8, it is easy to find that a concentration of 18 mg/l of suspended solids corresponds to a density change of 0.011 kg/m$^3$. Therefore, it can be safely assumed that changes in density due to solids are produced mainly by the TDS. This statement is valid only for the set of measurements currently available.

Despite the correction for temperature given by 2.5, the influence of temperature was judged as almost negligible in that equation. Figure 2.8 depicts the evolution of the density in terms of the water temperature, with and without dissolved solids. *It is noteworthy that the increase of density due to the presence of dissolved solids overcomes the decrease of density due to temperature*. For example, compare the points pertaining to 5 and 10 °C; the existence of solids increases the density by about 0.5 kg/m$^3$, whereas the decrease due to temperature is below 0.18 kg/m$^3$.

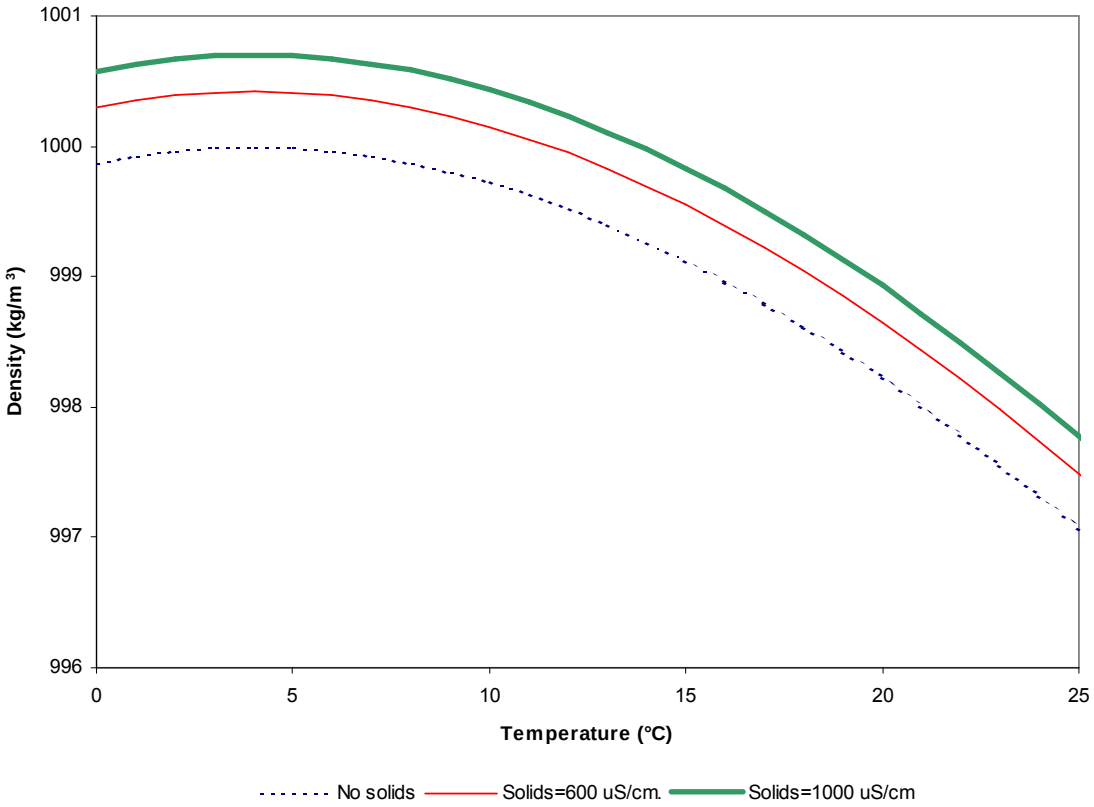


**Figure 2.8:** Water density distribution as a function of temperature and content of suspended solids

It is interesting to have an idea about the behavior of the different equations presented above. Figure 2.9a compares the performance of equations 2.3 and 2.4 in the prediction of the density. It can be seen that both formulas give very similar results in the range of interest.

Figures 2.9b and c in turn compare the performance of equations 2.5, 2.6 and 2.7 to predict the correction to the water density due to the presence of dissolved solids. To facilitate the comparison, equation 2.3 was employed for the computation of the variation of the density in the absence of dissolved solids, together with equations 2.5 and 2.6; similarly, equation 2.7 was linked to 2.4 for that purpose. Figure 2.9b shows the case pertaining to a suspended solids content given by 600 µS/cm and Figure 2.9c does the same for 1100 µS/cm. The conversion from µS/cm to TDS concentration was done through equation 2.1, for values of the constant equal to 0.5 and 0.75. The comparison shows that there are some discrepancies among equations 2.5 and 2.6 (which are very similar), with equation 2.7. This is a consequence of the different substances used by the different authors in the tests; the discrepancies are not so important when 0.75 is used for the constant and when the dissolved solids content is not too high. The discrepancies are bigger for larger dissolved solids contents.

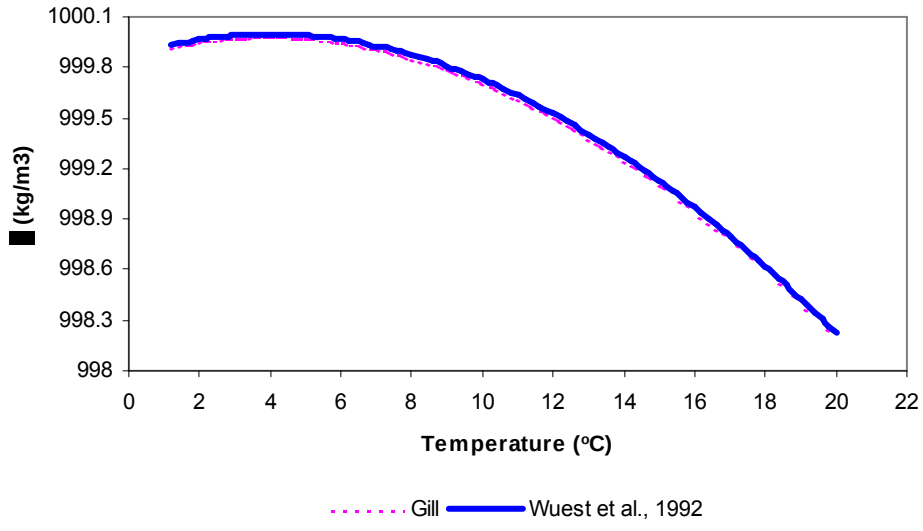


**Figure 2.9a:** Comparison between equations 2.3 and 2.4

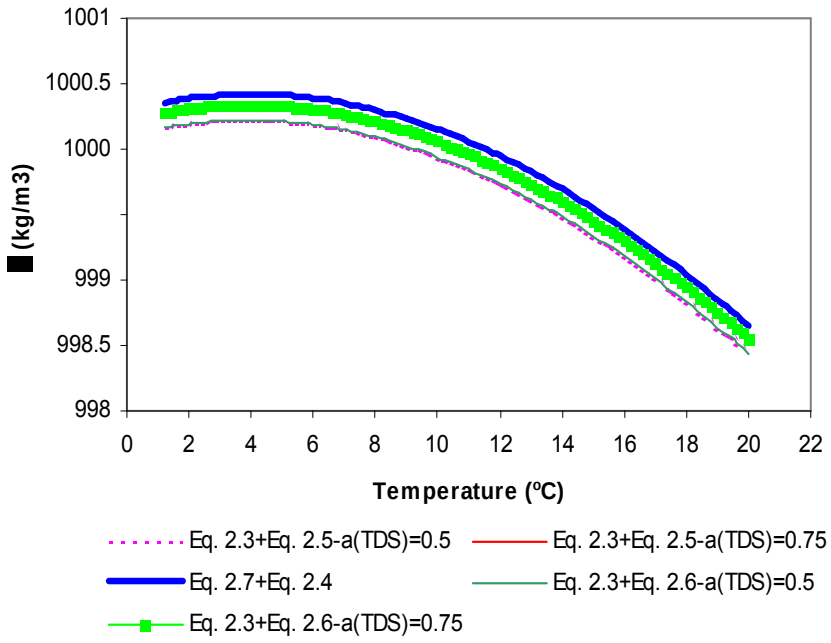


**Figure 2.9b:** Comparison among equations 2.5, 2.6 and 2.7 for a dissolved solids content of 600 µS/cm

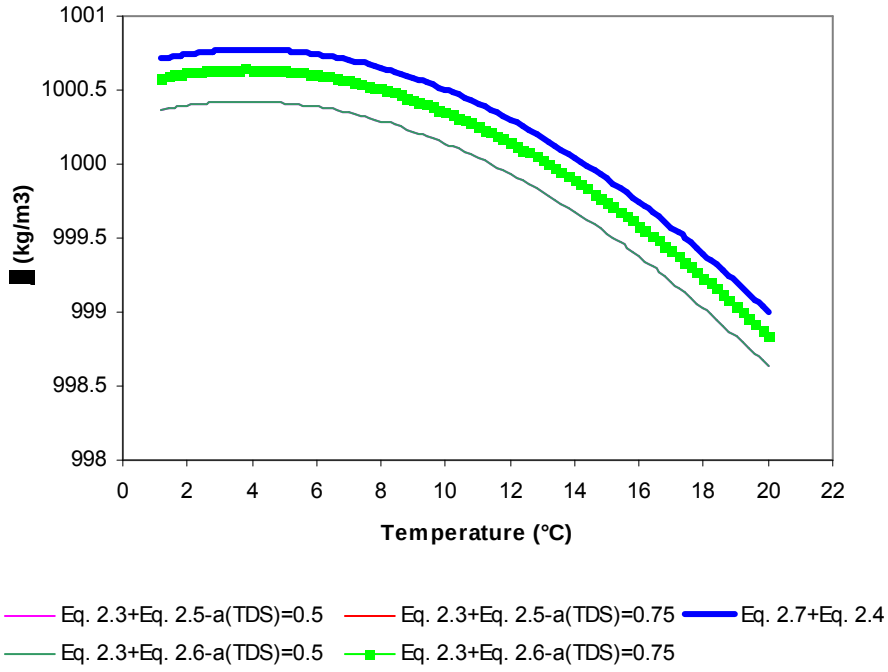


**Figure 2.9c:** Comparison among equations 2.5, 2.6 and 2.7 for a dissolved solids content of 1100 µS/cm

In order to convert the measured values of temperature and conductivity in the CR, equations 2.4, 2.7 and 2.8 were used, mainly due to their simplicity. These equations were applied to the observations available. Figures 2.10a-g show the results for different cross sections. From all the Figures, the same stable stratified pattern is clearly noticed. This means that, *after this conversion, there is no doubt that stable stratification dominates the CR throughout its length, despite the presence of "unstable" water temperature distributions in the vertical*. The maximum density differences oscillate between 0.5 and 1 kg/m$^3$. These would yield excess fractional densities ($\Delta\rho/\rho$) ranging from 0.0005 to 0.001.

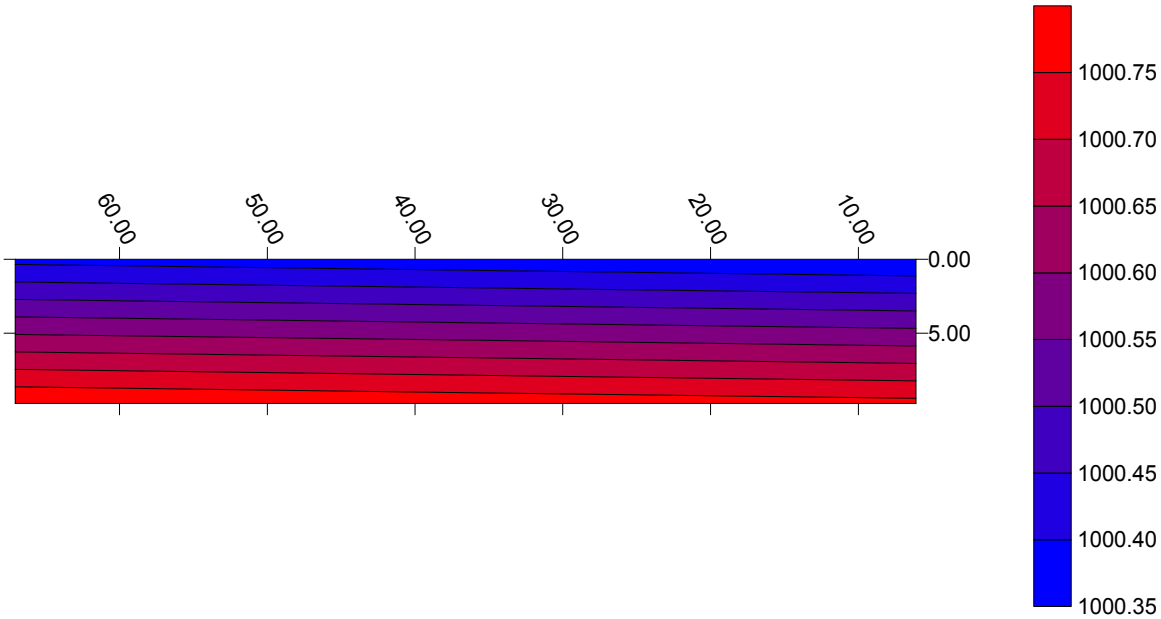


**Figure 2.10a:** Density distribution at Lake Shore Drive (03/19/98)

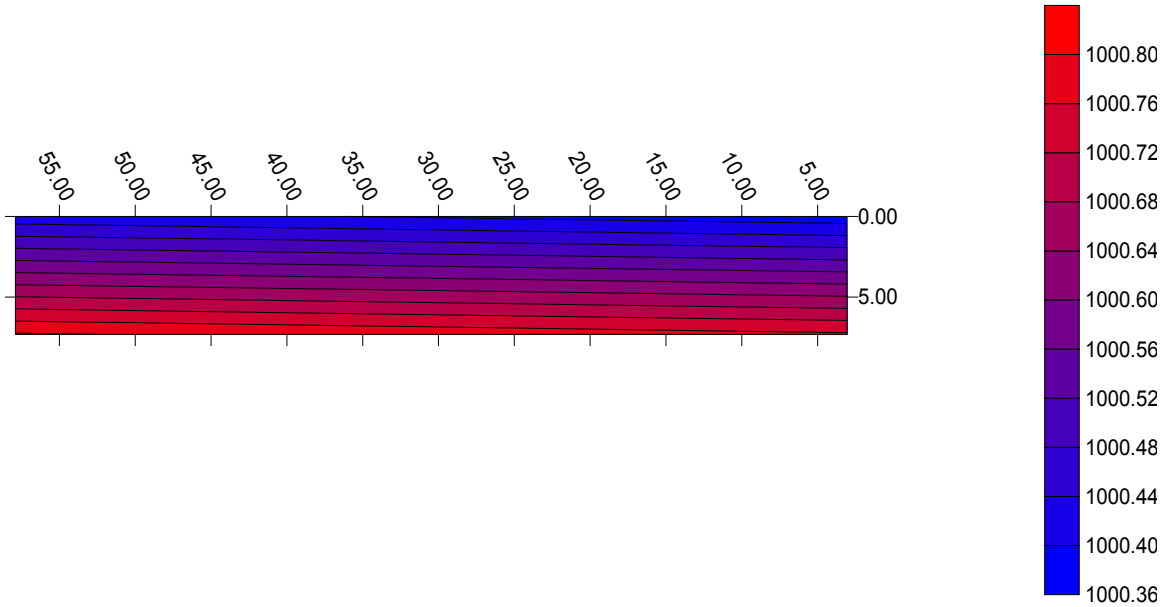


**Figure 2.10b:** Density distribution at Columbus Drive (03/19/98)

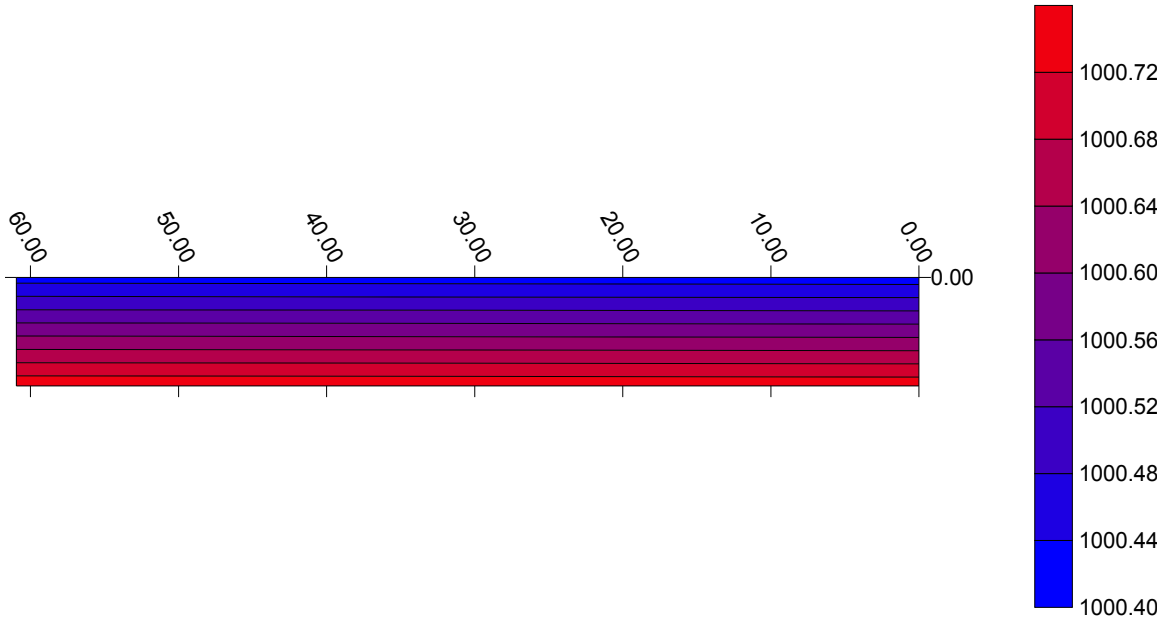


**Figure 2.10c:** Density distribution at Michigan Avenue (03/19/98)

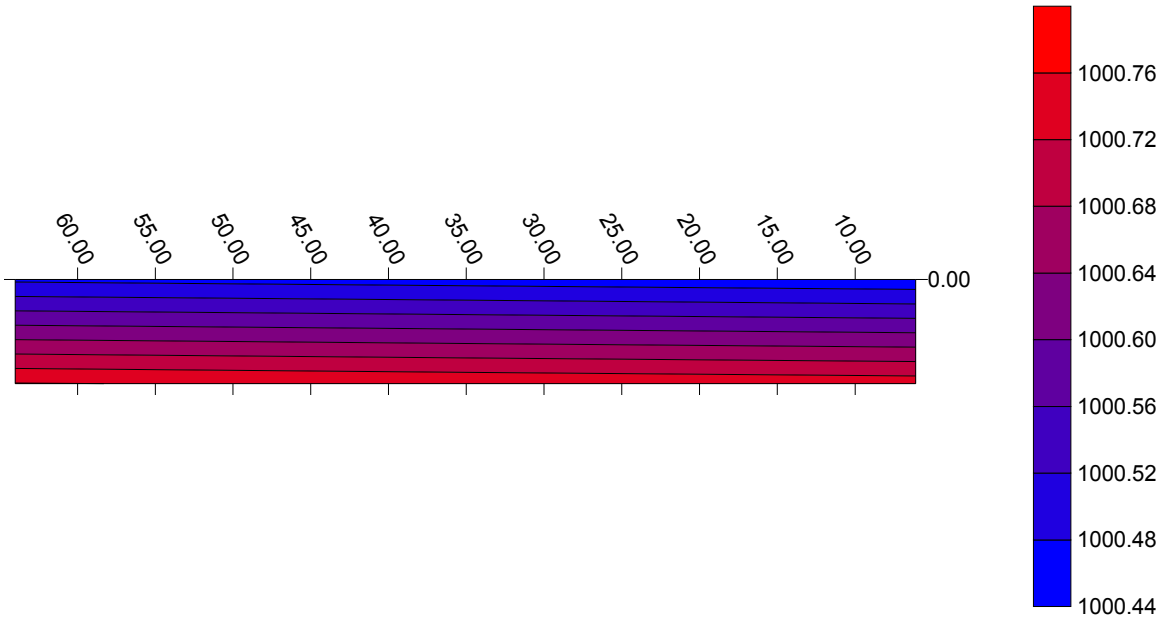


**Figure 2.10d:** Density distribution at Wabash Avenue (03/19/98)

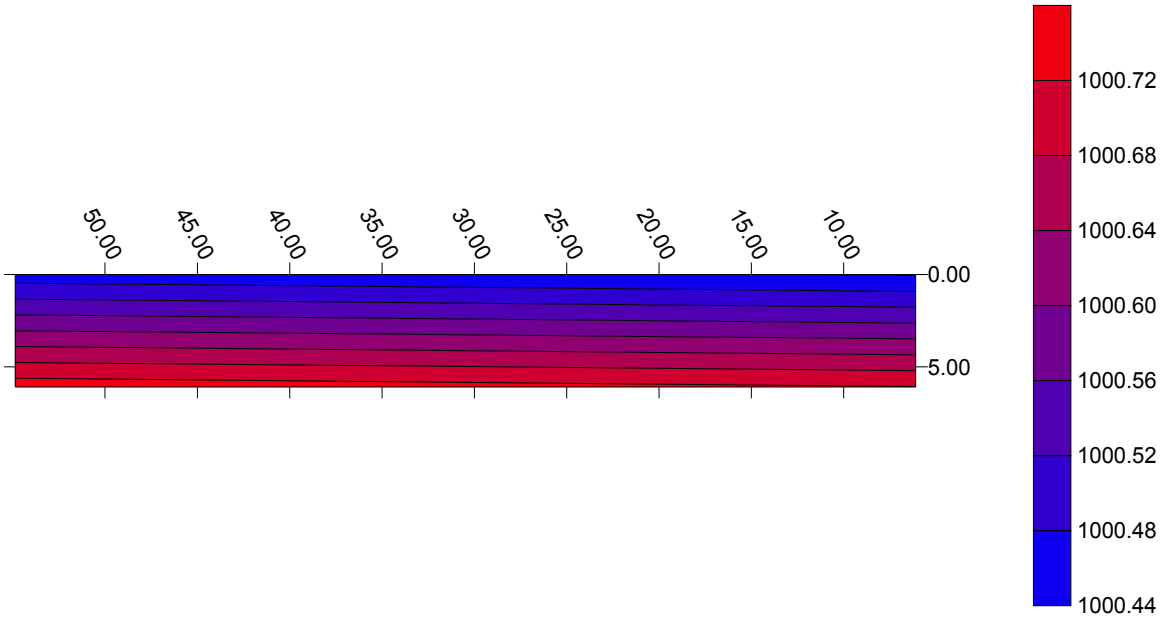


**Figure 2.10e:** Density distribution at State Street (03/19/98)

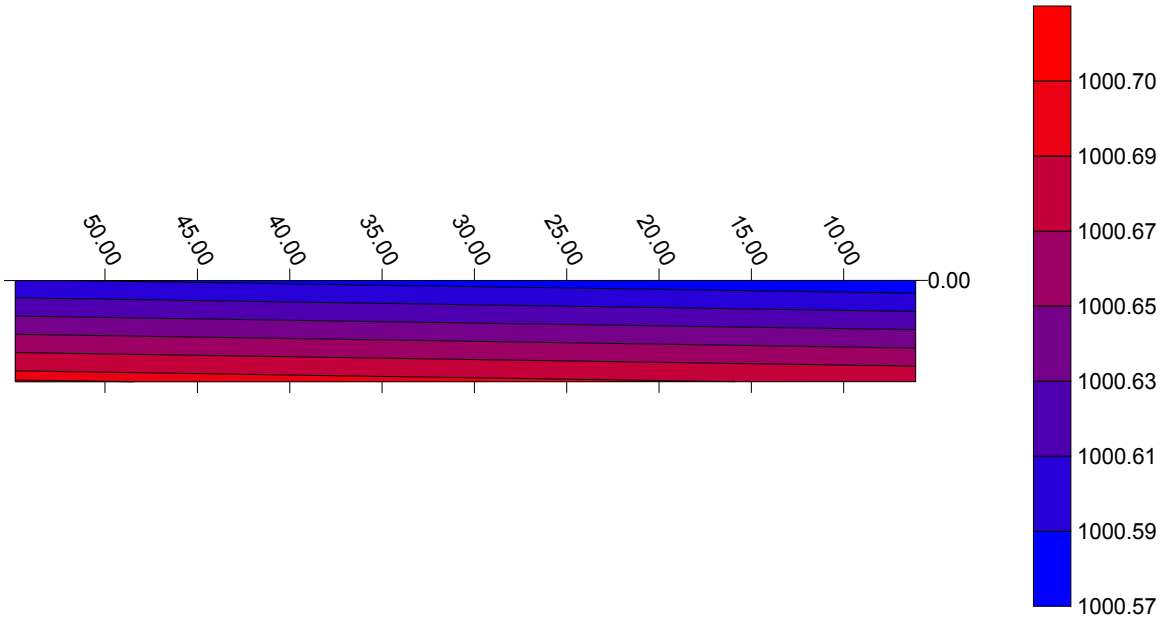


**Figure 2.10f:** Density distribution at Franklin/Orleans Street (03/19/98)

## 2.5 CONSIDERATION OF WIND-INDUCED FLOWS

According to the shape of the vertical velocity distributions within the CR, it could be argued that they are the result of wind action. Figure 2.11 shows laboratory measurements for wind-induced flows (Bombardelli, 1999; Bombardelli and Menéndez, 1999). It can be seen that while the profiles are similar to those found in the CR, the magnitude of the maximum positive and negative velocities are totally different. In wind-induced flows, the maximum negative velocities are, in module, of the order of 0.2 times the water surface velocity, which does not hold for the measurements in the CR. If we also consider that the pattern in the CR was observed many times during the winter of 1998, *it becomes clear that wind action cannot be responsible for the observation of bi-directional flows*.

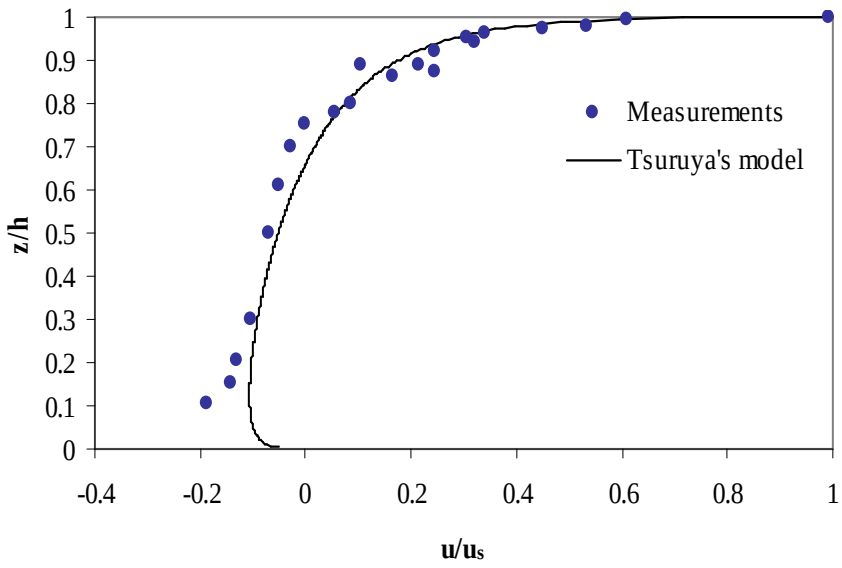


**Figure 2.11:** Vertical velocity profile for a wind-induced flow in a closed basin

## 2.6 CONCLUSIONS FROM ANALYSIS OF MEASUREMENTS

The analysis performed allows for the following main conclusions:

a) bi-directional flows, with a particular direction of the flow (lower velocities pointing to Lake Michigan) were observed several times during the winter of 1998 in the CR;
b) these bi-directional flows are concomitant with very small mean flows in the CR;
c) these flows were observed with the simultaneous occurrence of stable density stratification within the CR;
d) the NBCR and SBCR have poorer water quality than the CR and the water quality in the SBCR is in turn poorer than in the NBCR.

# CHAPTER 3
# THEORETICAL AND MATHEMATICAL MODELS FOR DENSITY CURRENTS IN THE CHICAGO RIVER

## 3.1 THEORETICAL MODEL

In the present analysis, only one portion of the NBCR and the SBCR is of interest. Towards the North, the analyzed domain comprises up to W. Chicago Ave. and, towards the South, up to Jackson Blvd.

Figure 3.1 shows the graphical representation of what it has been discussed in Chapter 1 in terms of the inputs to the system, based mainly on the information provided by the MWRDGC. The contributions from the lake are clearly stated, as well as the input from the North and the output towards South.

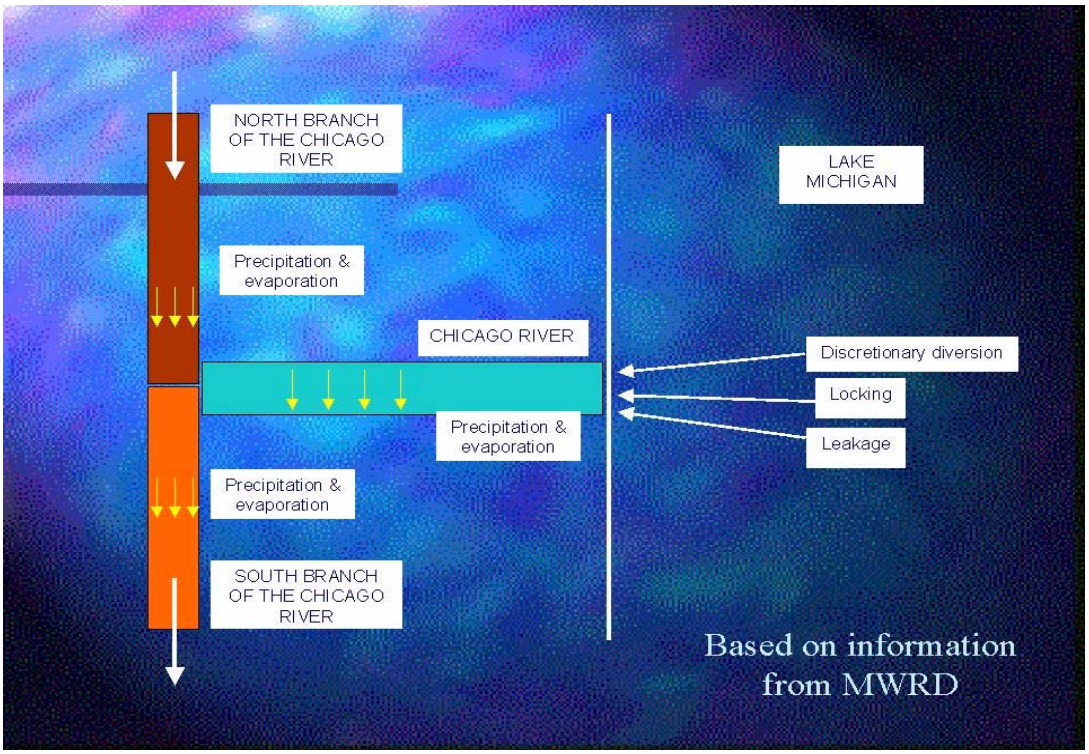


**Figure 3.1:** Schematization of the water inputs to the system

Based on Figure 3.1 and the conclusions drawn from Chapter 2, it is possible to obtain probable scenarios for summer and winter conditions in the CR. Thus, Figure 3.2 presents a potential scenario for summer (June through October), when locking activities are abundant and the discretionary diversion supplies water to the system. This scenario presents the possibility of denser water incoming from Lake Michigan and flowing along the bottom of the CR as a density current towards the junction. This water dilutes the incoming water from the NBCR at the junction and, consequently, the quality of the SBCR water is improved. To conserve mass, a countercurrent overflow would originate from the junction towards the lake. This scenario has not been measured by the USGS, but it is probable, according to the differences in water temperature and solid concentration between the lake and the CR. The presence, detected by the MWRDGC, of larger contents of suspended solids in Lake Michigan rather than in the CR supports the possibility of occurrence of such an event.

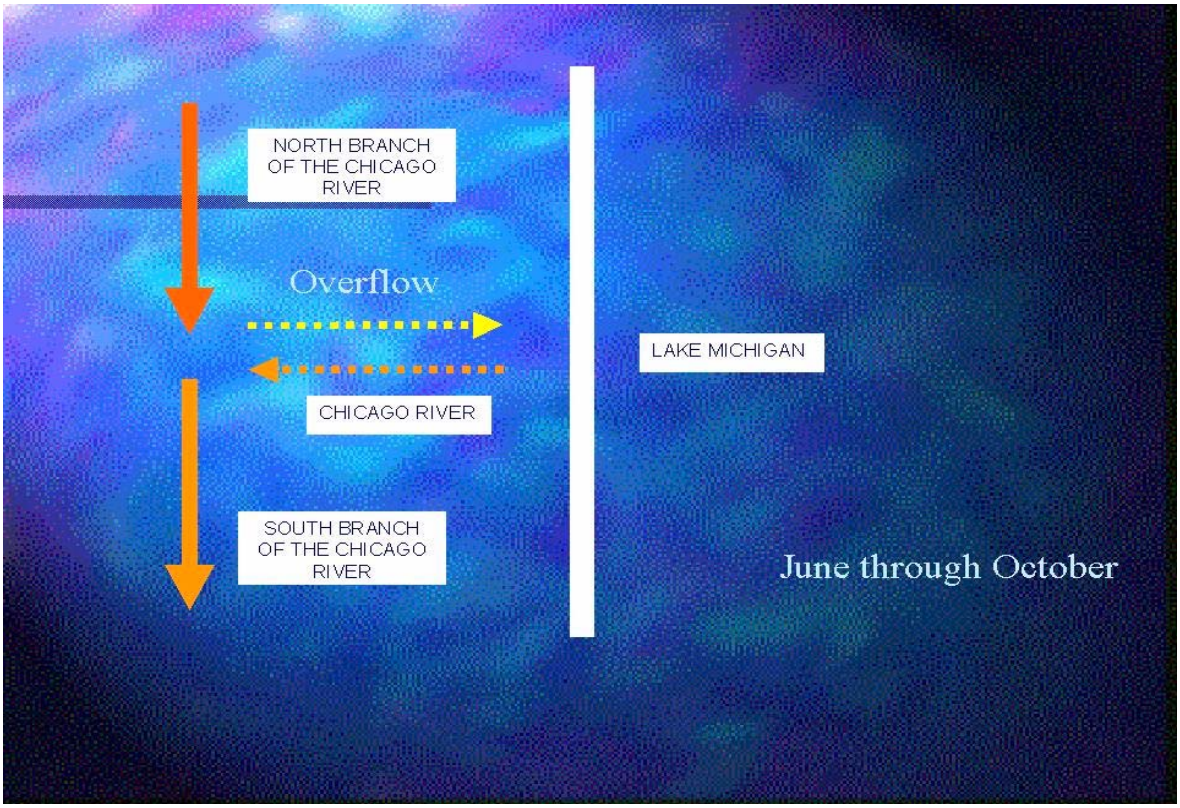


**Figure 3.2:** Potential scenario for summer months

Figure 3.3 shows the potential scenario for winter. In this case, the locking activities are minimal and the discretionary diversion has ceased. Therefore, there is no incoming beneficial effect from Lake Michigan. Under these circumstances, it is likely that water coming from the NBCR, with more content of solids and with larger temperatures (and consequently denser, as seen in Chapter 2), could plunge and move along the bottom of the CR as a density current. Again, to preserve mass, a countercurrent flow generates, causing an overflow taking water from the CR towards the junction. *Unlike the summer case, it is assumed herein that the conditions measured by the USGS in 1998 pertain to this scenario, and this gives rise to a theoretical model for the study of the phenomenon*. Next step consists in translating the model to differential equations and, finally, to certify that the adopted theoretical model for the development of density currents can explain the facts.

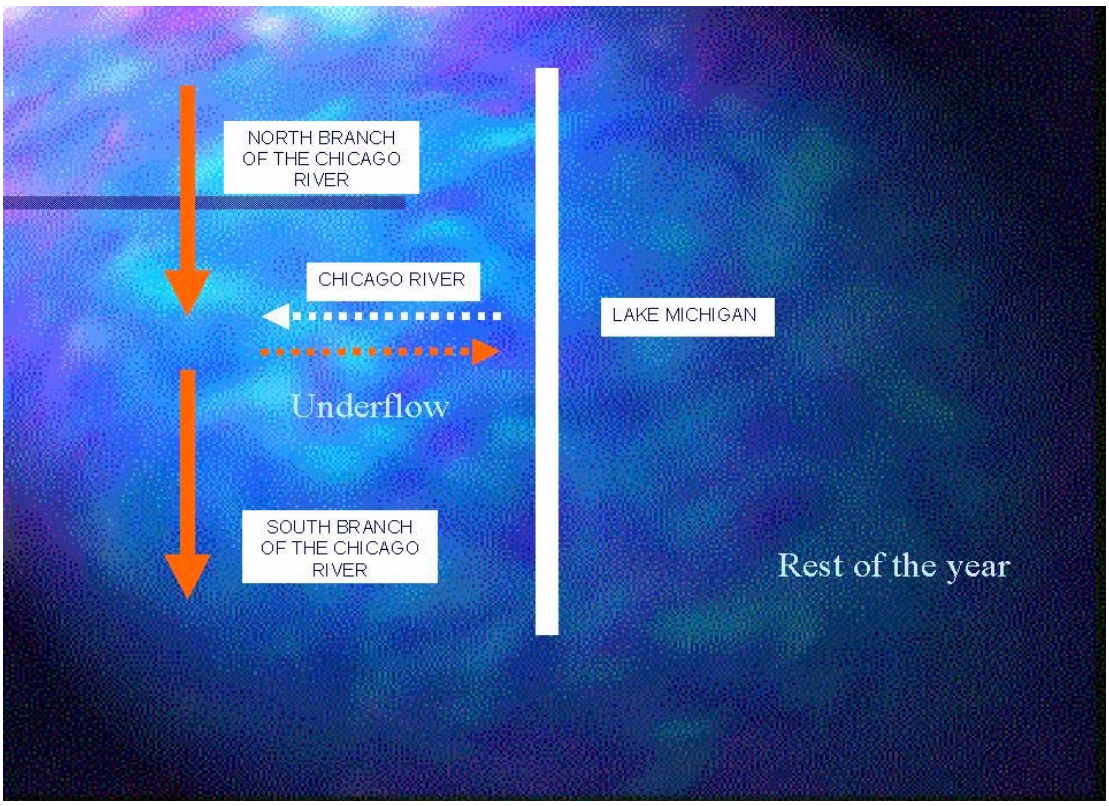


**Figure 3.3:** Potential scenario for winter months

It is interesting to note that, in these two ways, density currents are generated by density differences, but it should also be clear that their impact on water quality would be most detrimental during the winter months. The generation of density currents would also explain the marked differences in water color observed by the IDNR.

## 3.2 MATHEMATICAL MODEL FOR THE COMPUTATION OF DENSITY CURRENTS

The vast majority of the existing computational models for the study of density currents in water environments is one-dimensional (1-D), layer-averaged in the coordinate perpendicular to the direction of motion. Choi and García (1995) (see also Choi (1996)) presented a numerical solution of the 1-D, layer-integrated, theoretical model of turbidity currents, through the use of a dissipative-Galerkin (i.e., Petrov-Galerkin) finite element method. Recently, Bradford and Katopodes (1999a and 1999b) used the finite-volume method to solve a similar problem. The conservation equations solved in the above efforts were those for fluid mass, streamwise momentum and suspended sediment.

In two-dimensions, the first numerical efforts can be traced back to a paper by Daly and Pratch (1968). These authors used the marker-and-cell method in the solution of the Navier-Stokes equations (using the Boussinesq approximation) and a solute transport equation. Mitchell and Hovermale (1977) investigated the front of thunderstorms through numerical techniques, solving equations similar to the ones referred to above. Similar interesting studies were presented by Thorpe et al. (1980), Crook et al. (1985) and Haase and Smith (1989) (all of them related to atmospheric density currents) and Straka et al. (1993). Some authors have presented a 2-D solution based in multiple layers (Ben-zhao and Xin-rong, 1996).

In the present problem, the existing conditions at the CR, with all the 3-D geometric details and the features of the flow, suggest that using a 3-D model to capture all spatial variability and complexity would be most appropriate.

Herein, a viscous flow mathematical model for density currents is proposed, as follows:

a) Conservation of momentum:

$$\frac{\partial u_i}{\partial t} + \frac{1}{V_F}\left\{(u\ A)_j\ \frac{\partial u_i}{\partial x_j}\right\} = -\frac{1}{\rho}\frac{\partial p}{\partial x_i} + G_i - \frac{1}{\rho\ V_F}\ ws_i + \frac{1}{\rho\ V_F}\ \frac{\partial}{\partial x_j}\left[(A\ \tau_i)_j\right] \tag{3.1}$$

b) Mass conservation:

$$\frac{\partial (u\ A)_j}{\partial x_j} = 0 \tag{3.2}$$

c) Density:

$$V_F\ \frac{\partial \rho}{\partial t} + \frac{\partial\ \left[(u\ A)_j\ \rho\right]}{\partial x_j} = 0 \tag{3.3}$$

where:

$u_i$ : velocity component in the i-th direction (i goes from 1 to 3)

$x_i$ : spatial coordinate in the i-th direction

$p$ : pressure

$V_F$ : fractional volume open to flow

$A_i$ : fractional area open to flow

$\rho$ : local density

$G_i$ : body accelerations (coming from body forces)

$\tau_{ij}$ : viscous stresses

$ws_i$ : wall shear stress

It is interesting to compute also how the free surface position varies with time. This can be done through the solution of the following equation:

$$\frac{\partial F}{\partial t} + \frac{1}{V_F}\left\{\frac{\partial\left[F\ (u\ A)_j\right]}{\partial x_j}\right\} = 0 \qquad (3.4)$$

in which the variable $F$ defines the volume of fluid fraction (see Appendix 2).

The standard Newtonian constitutive relation was used to represent the fluid behavior in terms of the viscous stresses, keeping in mind that the concentration of dissolved, and mainly suspended, solids is too small to affect inertial terms.

It is important to note that the content of suspended solids in the CR is quite low; consequently, settling phenomena are not expected to occur based on the observations available. Therefore, no correction for settling velocities to the above equations is needed. At the same time, the equations are intended to explain the phenomenon (i.e., density currents), with a relatively fast time scale when compared to the settling velocity of the suspended solids.

It is also important to note that viscous flow models explain accurately the behavior of density currents in laboratory conditions. This observation is supported by the evidence presented in some previous papers, detailed above, and by the experience at the VTCHL (García and Bombardelli, unpublished report). In field situations, however, turbulence could “a priori” play a more important role. Present evidence would indicate that viscous flow models are accurate enough to predict also field situations.

No thermodynamic effects were included in these simulations at this stage; in future efforts this could be analyzed. At this stage, the adopted model seems to provide a plausible description of the density current phenomenon.

# CHAPTER 4
# NUMERICAL MODEL FOR DENSITY CURRENTS IN THE CHICAGO RIVER

## 4.1 NUMERICAL MODEL. PREVIOUS TESTS

Equations (3.1) to (3.4) were solved using FLOW-3D®, developed by Flow Science, Inc., Los Alamos, USA (FLOW-3D® User's Manual, 2000). Some details of the model are presented in Appendix 2. This code was recently tested at the VTCHL in many cases, with turbulent flows in hydraulic structures and streams (see Bombardelli and García, 1999; Caisley et al., 1999; Bombardelli et al., 2000; Rodríguez et al., 2000).

In order to certify that the above theoretical model, numerically integrated by FLOW-3D®, accurately predicts the motion of density currents, two tests were done. One of them relates to the experiments by Lin and Mehta (1997) and the other one is referred to the experiments done by Alahyari and Longmire (1996). Lin and Mehta studied experimentally the transport and sedimentation in laboratory basins, trying to obtain insight to the problem usually observed in marinas. In turn, Alahyari and Longmire tested experimentally the behavior of three-dimensional (3-D) density currents in a basin shaped like a circular sector. In Appendix 3, the details and results of the simulation for the tests of Lin and Mehta are presented, which show a very satisfactory description of the phenomenon. The same level of agreement was also obtained for the tests of Alahyari and Longmire, but this comparison is not included in this report.

## 4.2 SCENARIO FOR THE COMPUTATIONS

The scenario for the computations was based on the discussion performed in Chapter 2 and pertains to *winter conditions*; summer conditions could be analyzed as well, but this was not pursued at this stage. This means that *the selected scenario considers null flow from Lake Michigan into the CR*. Also, in this scenario, *the NBCR*

*and the SBCR are supposed to have a uniform density throughout the analyzed reach, equal to* $\rho_{high}$. This hypothesis is partially justified by the measurements provided by the MWRDGC and explained in Chapter 2. In turn, *the CR is assumed to have a lower density than the density in the North and South branches (* $\rho_{low}$*)*. Initially, it is supposed that there is an abrupt change of density at the junction and, at t=0 seconds, the system is left to evolve.

Two analyses were performed: first, an idealized domain was employed, in order to gain understanding about the flow and to address the influence of the geometry, computational mesh characteristics and boundary conditions onto the numerical solution; then, the real bathymetry was used.

### 4.2.1 Computations for the idealized case

#### *4.2.1.1 Domain, geometry and mesh characteristics*

The idealized domain comprised a parallelepiped of 2000 m in the x-direction and 2100 m in y-direction, which roughly represents the analyzed domain. In the vertical, the domain included 8 m, with water levels at about 7 m from its bottom. Figure 4.1 shows a schematic of the idealized domain.

The geometry was introduced into the numerical model through FLOW-3D® solid modeler; the bottom of the river was assumed to be horizontal. The CR was represented with a width of 70 m, whereas the branches were given a width of 75 m.

350,000 finite volumes were used for this computation (not all of them participate in the computation, provided some of them are blocked) with densification in concomitance with the riverbeds. This large volume of computation, together with an unsteady flow run, made the computational effort important.

### *4.2.1.2 Initial and boundary conditions*

The densities were set as: $\rho_{high}$ = 1007 kg/m$^3$ and $\rho_{low}$ = 1000 kg/m$^3$; the higher density was larger than the values seen in the CR, but the test was considered appropriate to identify the response of the system.

Constant velocities (input for the NBCR; output for the SBCR, going from North to South) were set as boundary conditions, with a value of 0.1 m/s. A difference in water levels of 0.1 m between the NBCR and the SBCR was also set. No inputs from buildings or precipitation were considered in these computations.

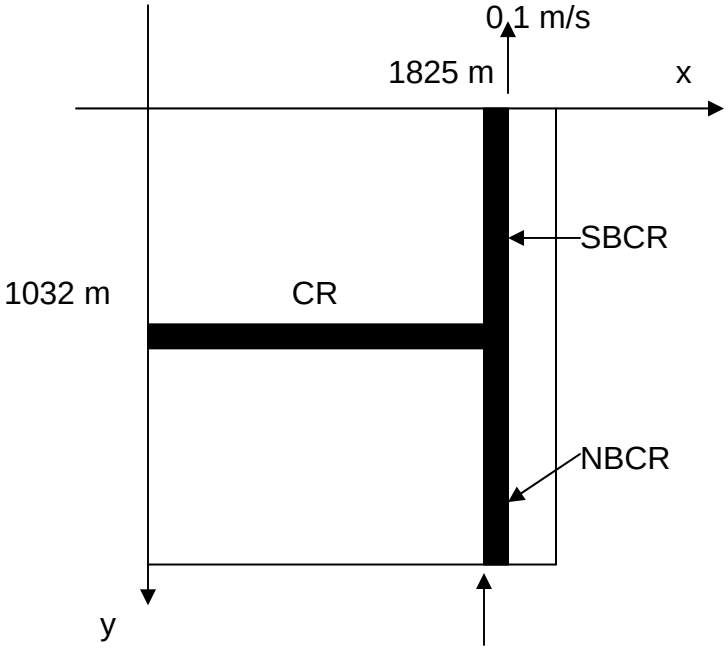


**Figure 4.1**: Schematization of the idealized domain

In order to ensure the input of denser water to the lower boundary of the NBCR, a small volume of water with that density has to be present close to the boundary (FLOW-3D® User's Manual, 2000).

### *4.2.1.3 Results*

First, the numerical runs allowed for the corroboration of the robustness of the computations for large domains. Sensible spatial steps were determined in order to guarantee both robustness and accuracy. Second, despite the fact of increasing the computational effort, the numerical integration of Equation 3.4 (related to the determination of the free-surface evolution in time) proved to be very beneficial for the correct description of the phenomenon.

*The numerical solution showed the formation of a density current that propagates along the bottom towards Lake Michigan*. Figure 4.2 shows a snapshot from the top of the front pertaining to 2100 seconds after the beginning of the computations. It corresponds to a horizontal plane at 35 cm from the bottom. A "separation" effect can be clearly identified; this separation later disappears as the front progresses and the flow reattaches to the river bank.

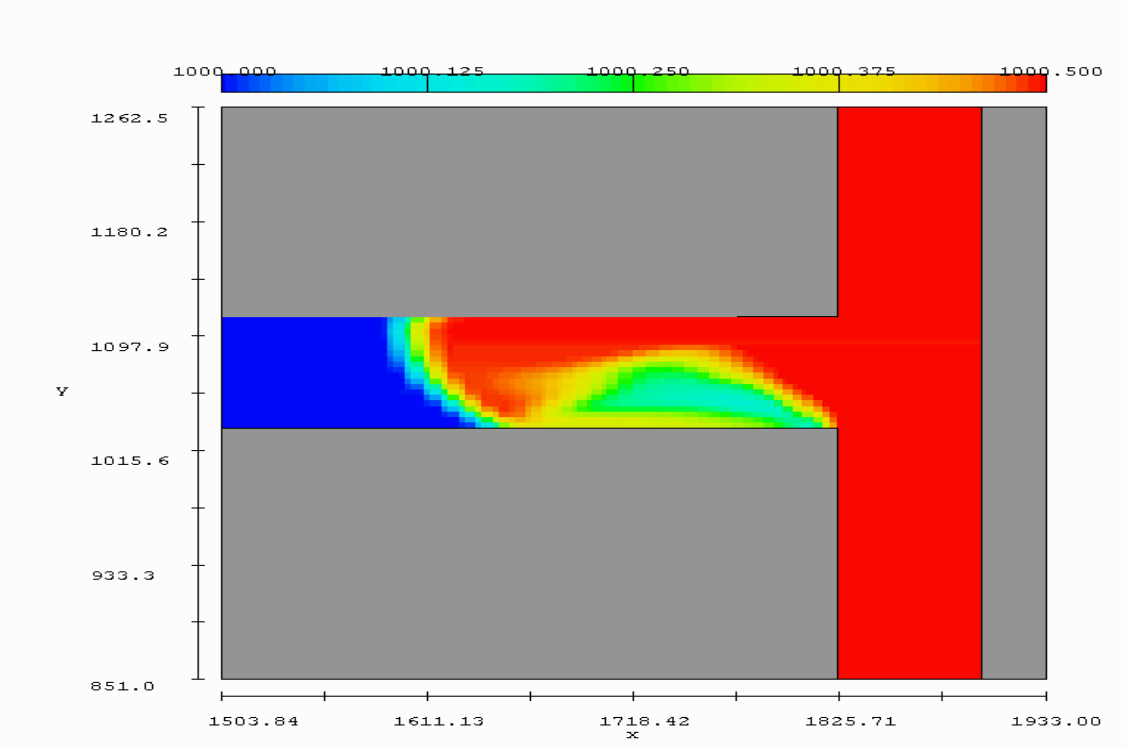


**Figure 4.2:** Snapshot of the numerical result for 2100 seconds (density contours in kg/m$^3$)

### 4.2.2 Computations with the real bathymetry

#### *4.2.2.1 Digital model for the real bathymetry, domain and computational mesh*

The real bathymetry was incorporated into the model through Stereolitography. In order to accomplish this task, *a methodology developed at the VTCHL was employed, which consists in a set of transformations that starts with the raw data coming from the surveys and finishes with the final determination of the STL file*.

The survey data used for the cross sections were obtained from an output of a previous model done with HEC-6. Staff from USACE supplied these data. Since these data were in English units, it was necessary to transform them to the metric system and relate them to an absolute datum. The first step in doing this was to create a reference point with 1000 latitude and 100 longitude. Based on this new reference coordinate system, all the other points were located on a longitude-latitude plane. The elevations were transformed to meters above sea level. The final output of this initial transformation is a data set of points with 3 coordinates: longitude, latitude and elevation above mean sea level. All these values were in meters and therefore the whole dataset was consistent.

The following step was to use the new dataset to generate a three-dimensional mesh to represent the area of interest (it is interesting to note that this mesh differs from the grid used for the computations; it only serves to the purpose of building a solid body).

Based on the results obtained with the idealized domain and following the studies that suggest that the adaptation length in open-channel flows is of the order of 20-40 times the flow depth, it was concluded that the influence of the boundaries on the flow at the junction is minor if they are located beyond 350 m. The portion used to generate the mesh (again, the mesh related to the geometry) corresponds to the following zones: NBCR between Chicago Avenue (river mile 326.41) and the junction (river mile 325.6);

SBCR between the junction and Adams Street (river mile 325.01); CR between Lake Shore Drive (river mile 326.94) and Franklin Avenue (river mile 325.57). The method used to obtain surfaces from the cross sections was triangulation, so as to end up with a set of geodesic triangles. Once the geodesic model was obtained, a simple interpolation was done to transfer the triangles to a rectangular mesh. Thus, the survey was transformed to a "bathymetric model". This final rectangular mesh has a big set of points. The resolution used was 1 meter x 1 meter in the XY plane (Tecplot™ was used to develop this task). Figures 4.3 and 4.4 show an isometric view and contour lines of the final bathymetry model obtained. The vertical scale is exaggerated 30 times.

The final transformation consists in converting the interpolated values to an AutoCAD® file. Once inside AutoCAD®, a solid is generated (i.e., the values pertaining to a surface are converted to a solid body). Later, this body is exported as an STL file. This file is input directly to FLOW-3D®.

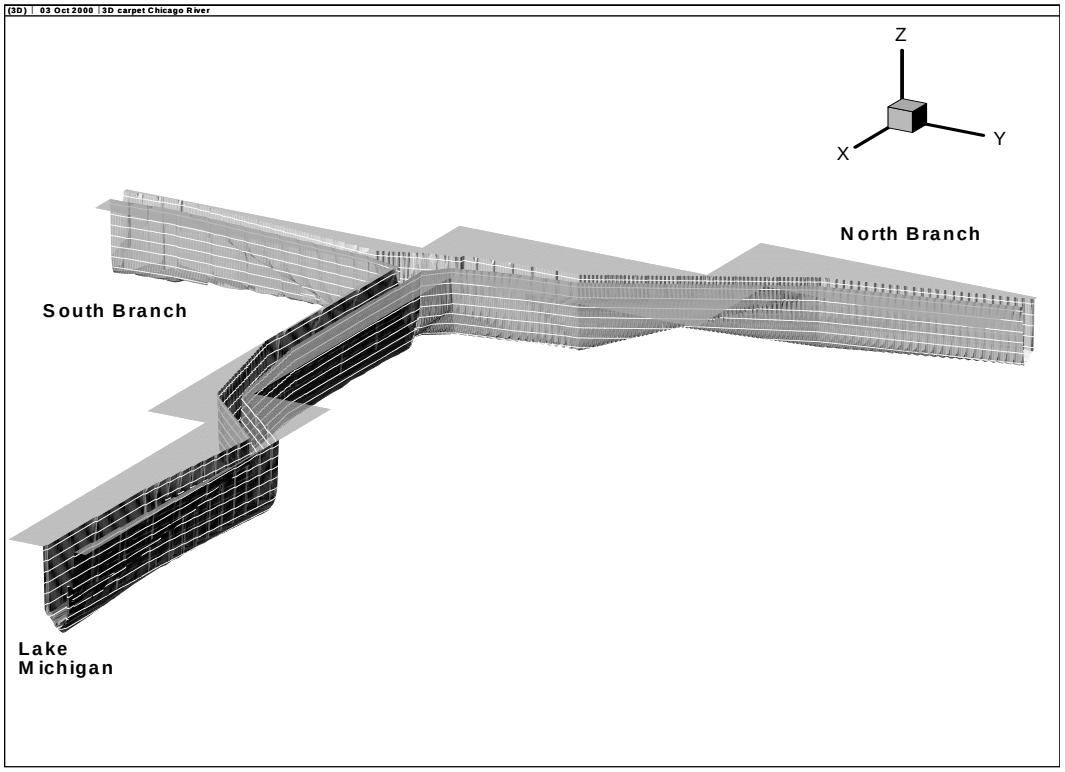


**Figure 4.3:** Isometric view of the bathymetry model

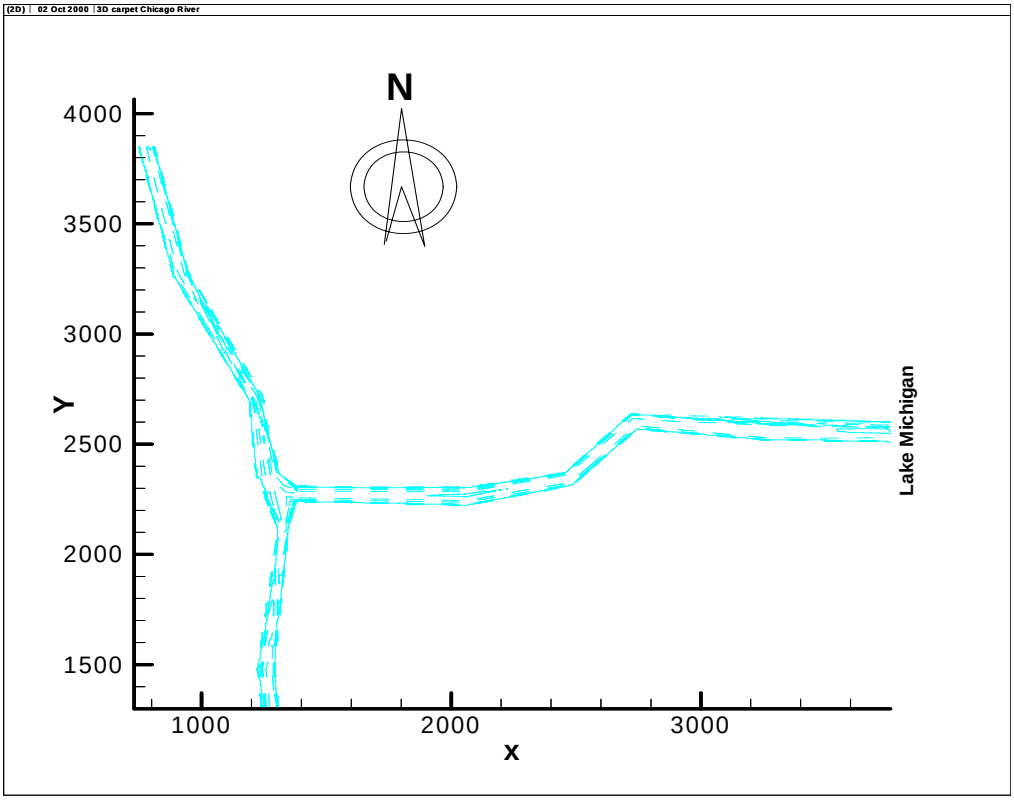


**Figure 4.4:** Contour plots of the bathymetry model

Figure 4.5 depicts a plain view of the domain and the employed computational mesh, which included 540,000 finite volumes. This computational mesh was obtained trying to follow the more active zones of the domain. In the Figure, the denser fluid is displayed in red and the lighter fluid in blue.

### *4.2.2.2 Initial and boundary conditions*

A difference in water levels was set between the NBCR and the SBCR boundaries; the density entering to the NBCR was the denser one (this has to be specified explicitly in the model, as explained previously). The values of the densities were as follows: $\rho_{high}$ = 1002 kg/m$^3$ and $\rho_{low}$ = 1000 kg/m$^3$, which reflect the conditions within the system. No inputs from buildings or precipitation were considered. The

boundary condition at Lake Michigan was impenetrability or zero flow through. No-slip conditions were set in the solid boundaries.

#### *4.2.2.3 Results*

Several runs were performed changing different parameters until the optimum conditions were attained. In the final run, 5 hours of real time were simulated, demanding about 150 hs to be completed, which illustrates the computational effort.

Figures 4.6 to 4.9 show top views, taken at a level close to the bottom of the river, of the density field. *It can be seen that there is a front that propagates with a variable speed towards Lake Michigan*. Transition zones of variable density lie between the limiting values. In turn, Figures 4.10 and 4.11 show lateral views (in vertical planes) that provide clear evidence of the propagation of a density current from the junction. Figure 4.12 shows a typical vertical velocity distribution in the CR. The order of magnitude of the computed velocities agrees well with the measured ones.

Figures 4.13 and 4.14 show the density distribution in Franklin/Orleans Street and State Street cross sections. *It takes about 1.7 hs for the front to reach State Street, but it takes much longer times to reach Lake Michigan, provided that the velocity of the front decreases in time (it is farther from its source). It is also noticeable that the thickness of the density current is of about 3 m (9 ft), which represents 43 % of the depth and agrees well with the measurements undertaken by the USGS. Additionally, the distribution of density predicted by the model is uniform throughout the cross section, as measured in the CR. Notice that this mechanism explains why the pattern of stratification repeats itself in the whole river, as observed by the USGS. Thus, it seems plausible to assume that the theoretical model, numerically integrated, gives a very clear cause-effect relation for the phenomenon observed in the CR*.

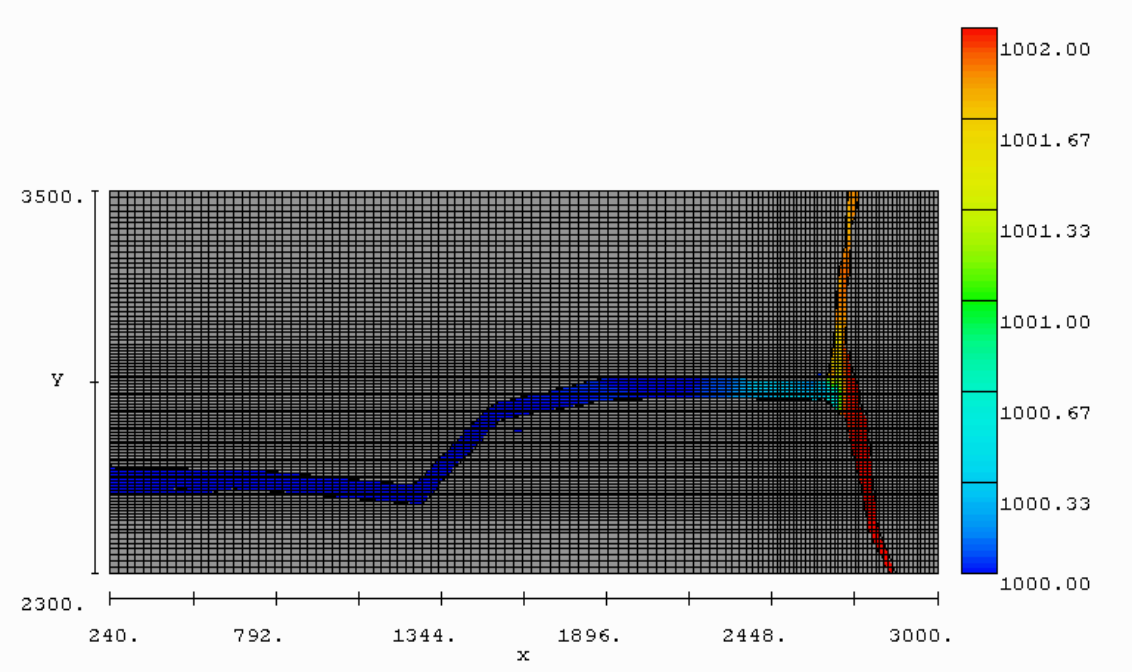


**Figure 4.5:** Final domain and computational mesh

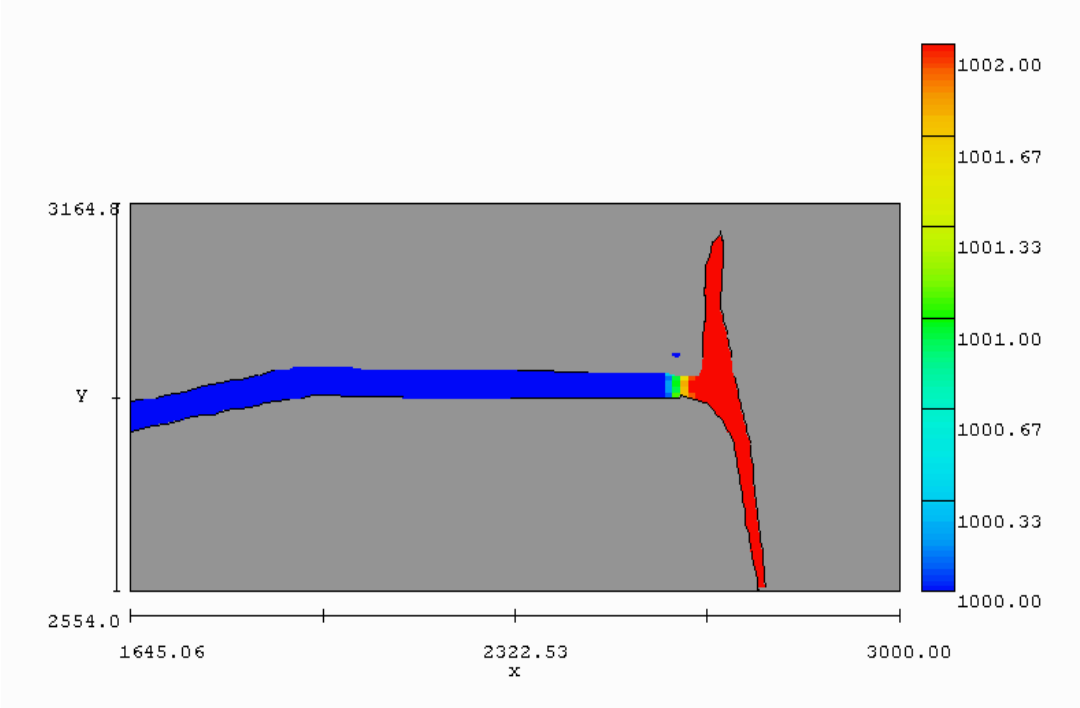


**Figure 4.6:** Close-up top view of computed density contours in the CR for 120 seconds of real time. This pertains to the upper part of the domain

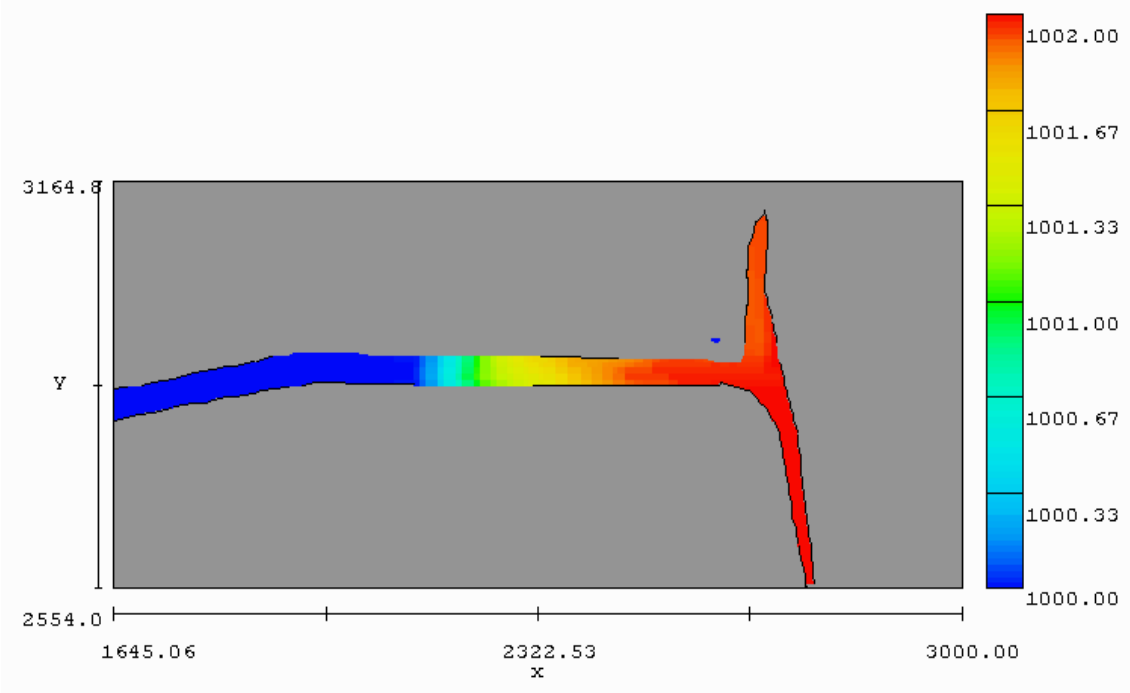


**Figure 4.7:** Close-up top view of computed density contours in the CR for 1 hour of real time. This pertains to the upper part of the domain

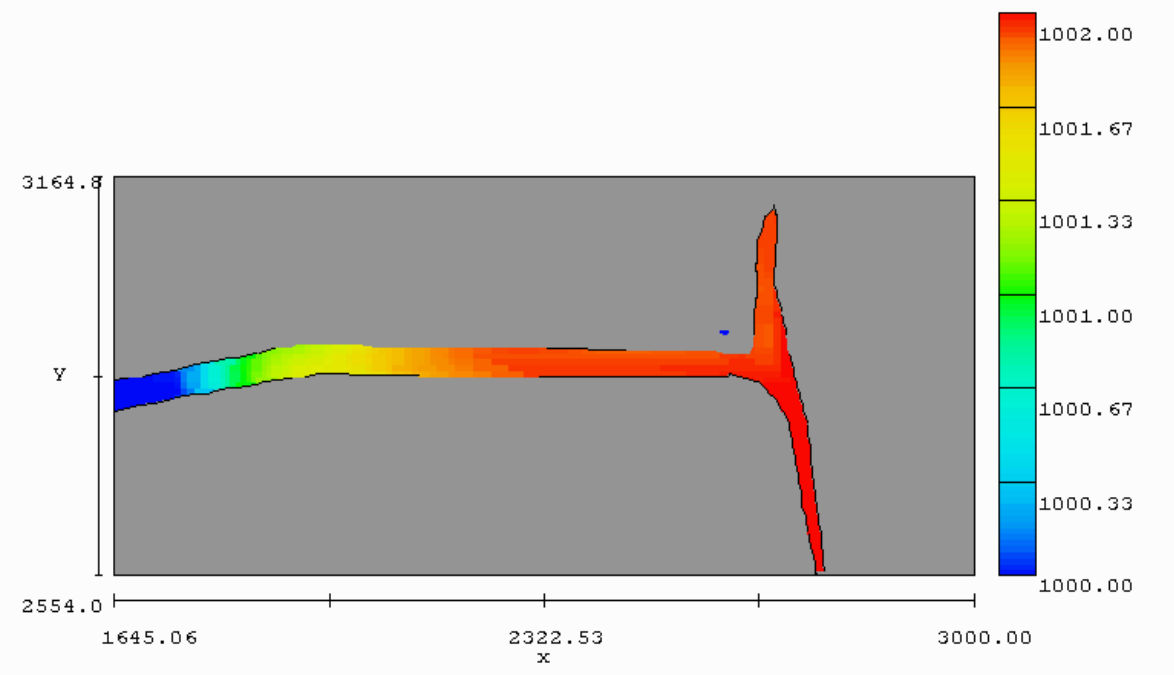


**Figure 4.8:** Close-up top view of computed density contours in the CR for 2 hours of real time. This pertains to the upper part of the domain

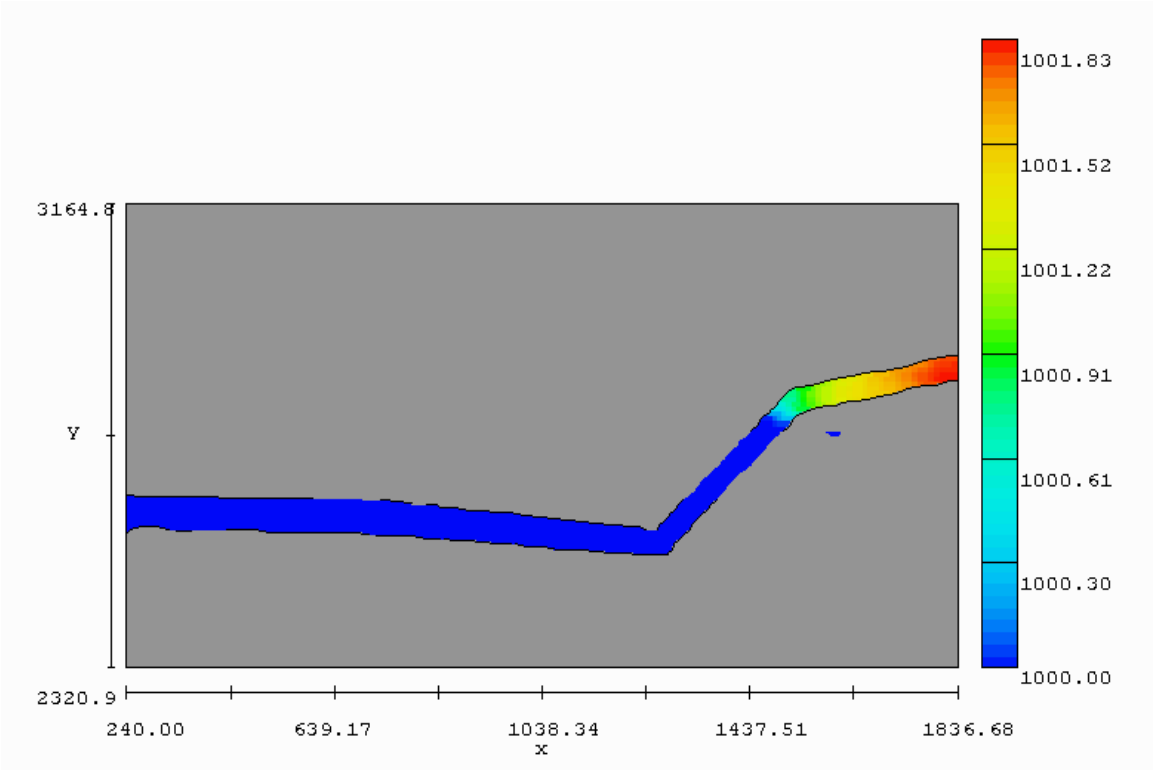


**Figure 4.9:** Close-up top view of computed density contours in the CR for 3 hours of real time. This pertains to the lower part of the domain

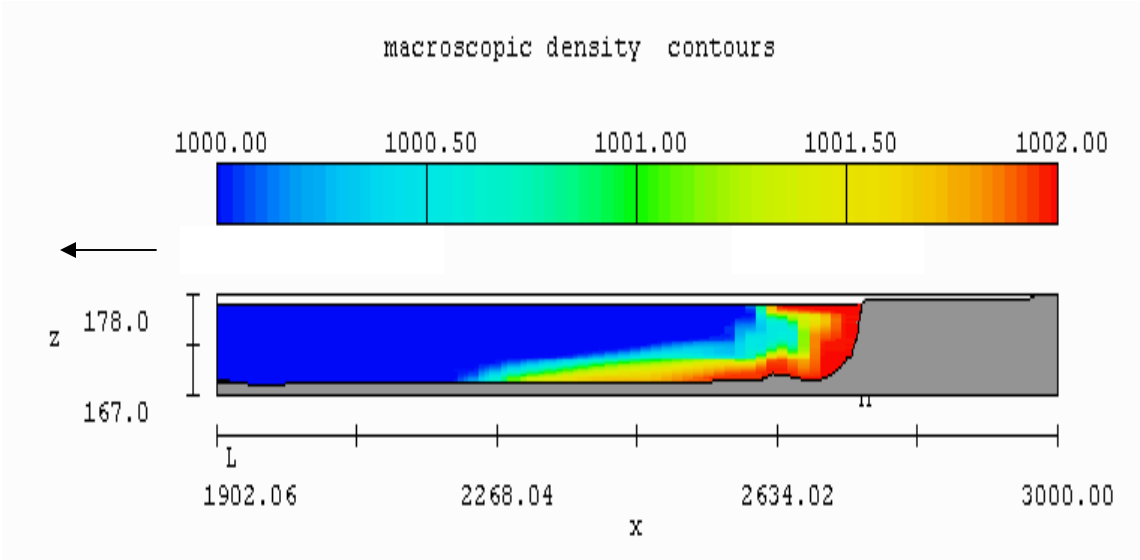


**Figure 4.10:** Close-up side view of computed density contours in the CR for 2600 seconds of real time

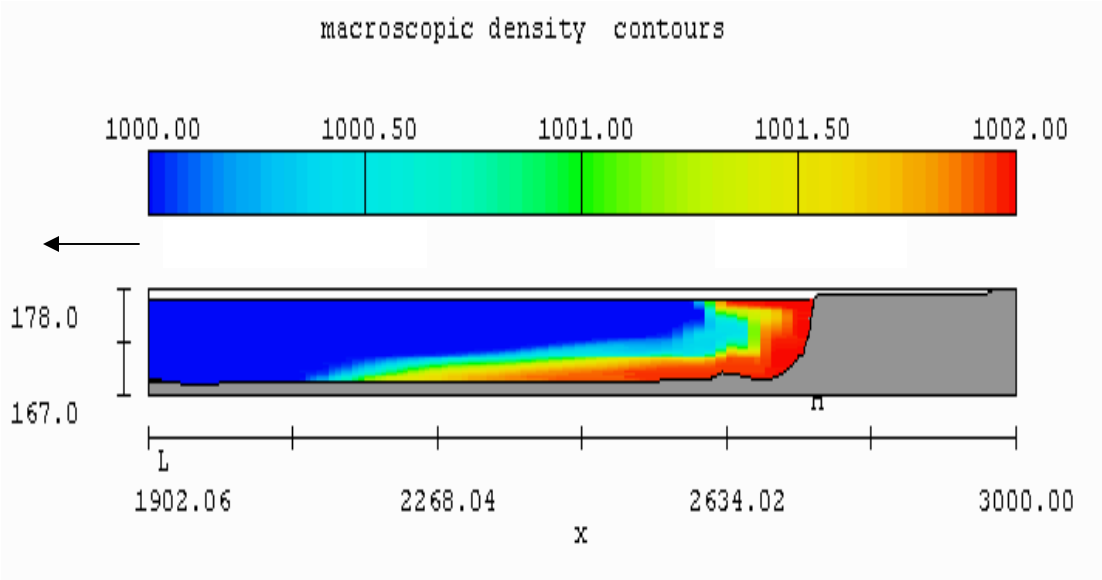


**Figure 4.11:** Close-up side view of computed density contours in the CR for 3600 seconds of real time

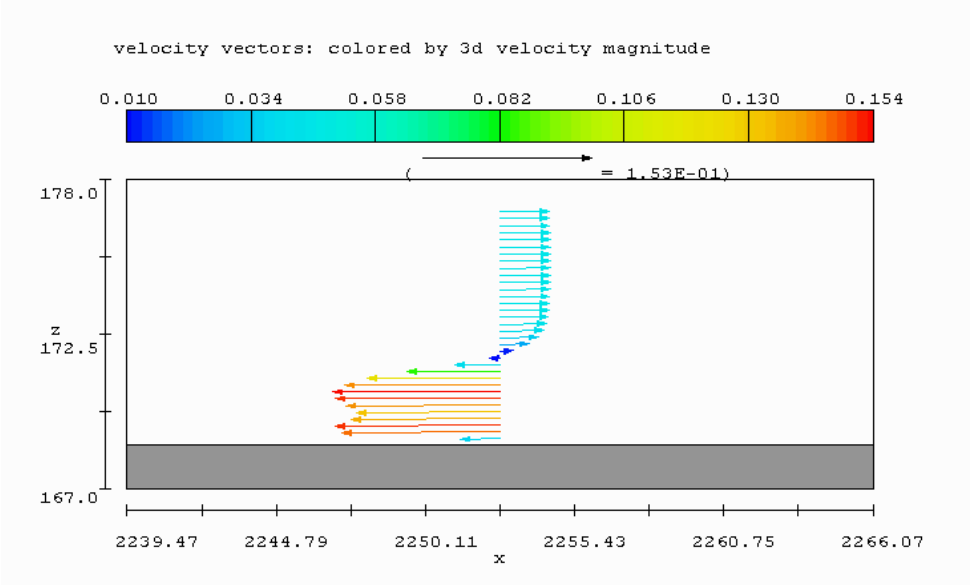


**Figure 4.12:** Vertical velocity distribution in the CR after 4400 seconds of real time at 450 m from the junction

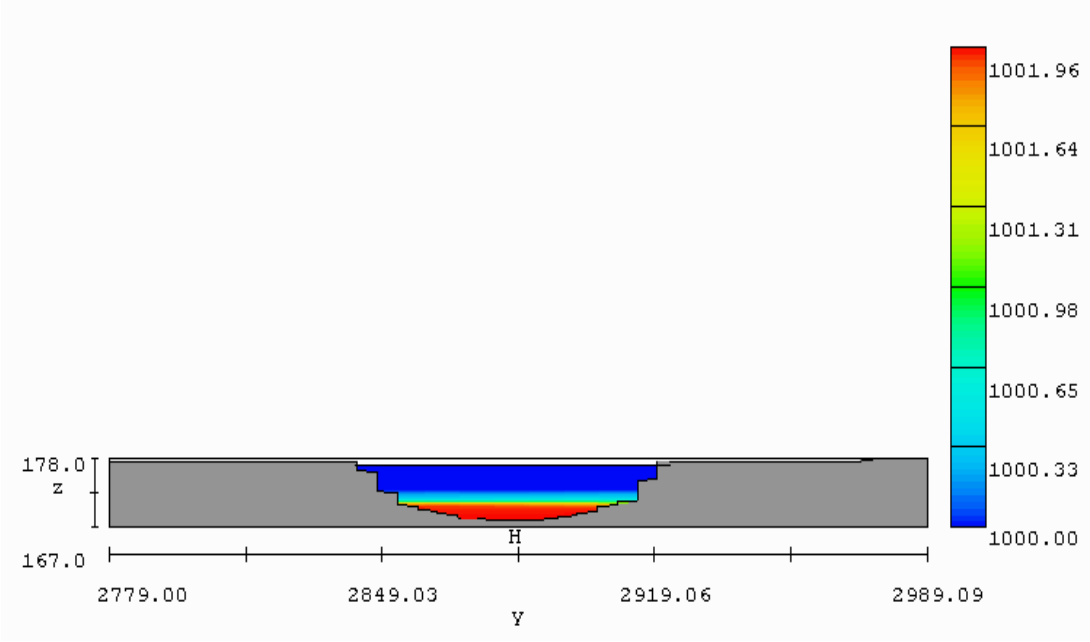


**Figure 4.13:** View of computed density contours in the CR at the cross section of Franklin Street

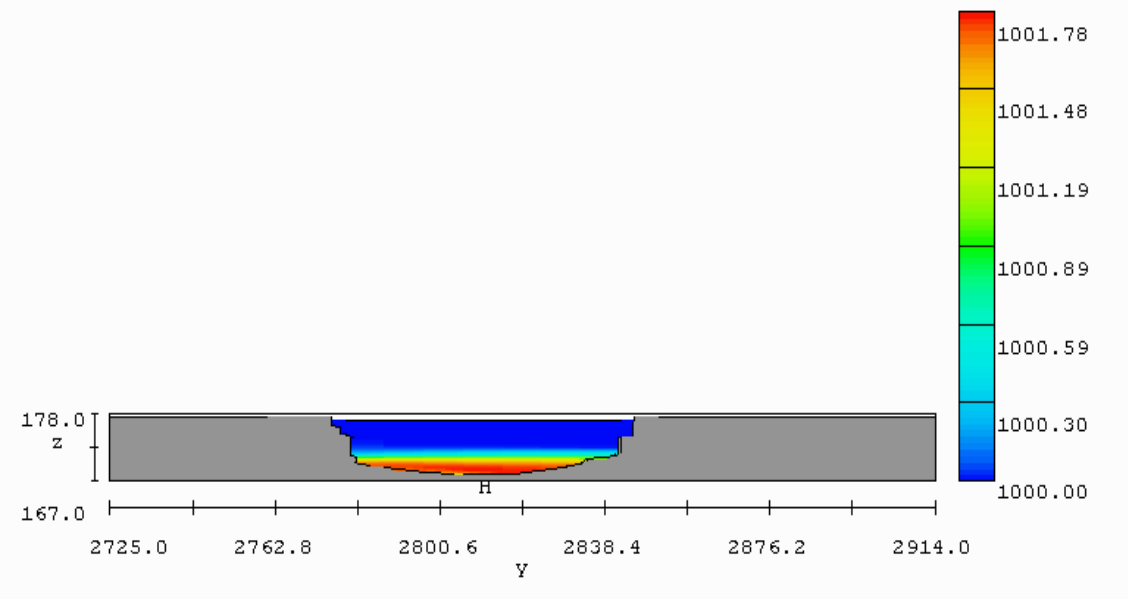


**Figure 4.14:** View of computed density contours in the CR at the cross section of State Street

# CHAPTER 5
# CONCLUSIONS AND RECOMMENDATIONS

## 5.1 CONCLUSIONS AND CONCLUDING REMARKS

The analysis undertaken until now leads to the following conclusions:

a) Preliminary numerical computations show that a mechanism based on the development of density currents in the Chicago River can be used to explain qualitative and quantitatively the behavior observed by the USGS in terms of vertical density distribution and bi-directional flow velocity profiles. These results suggest the meaningfulness of the theoretical model adopted.

b) The calculated density current presents a thickness of about 3 m (9 ft), which agrees well with the measurements obtained by the USGS.

c) More detailed field measurements are needed in order to definitely calibrate and validate, through the definition of more clear scenarios, the ongoing hydrodynamic computational model of the Chicago River and improve future model predictions.

d) More computational efforts are needed to study the evolution of the system under diverse conditions, such as wind, flow discharge (diversion) incoming from the lake, etc.

e) A thorough understanding of the river hydrodynamics will facilitate both the generation of sound recommendations and the formulation of effective rules for the operation of the system, including the pumping station recently constructed by the IDNR.

## 5.2 RECOMMENDATIONS

The above analysis leads to the following recommendations for measurements in the CR and its branches:

a) Velocity measurements (AVM and ADCP) + specific conductance + temperature + turbidity + concentration of suspended solids + water levels
    1. Possible stations in the Chicago River:
        i. Franklin/Orleans Street
        ii. Clark Street
        iii. State Street
        iv. Michigan Avenue
        v. Columbus Drive
        vi. Lake Shore Drive
    2. Possible stations in the South Branch of the Chicago River:
        i. Lake Street
        ii. Madison Street
        iii. Jackson Blvd
    3. Possible stations in the North Branch of the Chicago River:
        i. Kinzie Street
        ii. Grand Avenue
        iii. Chicago Avenue

b) Velocity measurements should be capable of resolving flow velocities every 10-15 cm in the vertical.

c) Temperature measurements should be taken on an almost continuous basis with the help of thermistor chains placed along the whole wetted perimeter of the cross sections recommended above.

d) Settling rates of suspended solids found in the water column, particularly in the North Branch of the Chicago River, should be determined.

e) A tracer study should be conducted by releasing rhodamine along the bottom of the North Branch of the Chicago River before the junction and doing measurements with a field fluorometer at different locations in the Chicago River.

f) Improved bathymetric information is needed in order to study the influence of local 3-D effects.

g) Field measurements and numerical modeling are also needed to understand the hydrodynamics of the system in the proximity of Lake Michigan. This could provide important information for the effective operation of the gates for water diversion from Lake Michigan as well as the recently constructed station for pumping water back into the lake.

## REFERENCES


[1] Alahyari, A. A., and Longmire, E. K. (1996). “Development and structure of a gravity current head.” *Experiments in Fluids*, Springer-Verlag, 20, 410-416.

[2] Ben-zhao, Z., and Xin-rong, S. (1996). “Finite layer model for 2-D thermal density flow in a channel.” *J. of Hydrodynamics*, China, Ser. B, 2, 85-91.

[3] Bombardelli, F. A. (1999). “A quasi-three-dimensional model to simulate wind-induced shallow-water flows.” MS Thesis, Universidad de Buenos Aires, Argentina (in Spanish).

[4] Bombardelli, F. A., and Menéndez, A. N. (1999). "A physics-based quasi-3D numerical model for the simulation of wind-induced shallow water flows.” *Proc. 1999 Int. Water Resources Engineering Conf.,* ASCE.

[5] Bombardelli, F. A., and García, M. H. (1999). “Numerical exploration of conceptual models for hydraulic jumps.” *Proc. World FLOW-3D® User’s Conf.*, Santa Fe, New Mexico, September 27-28.

[6] Bombardelli, F. A., García, M. H., and Caisley, M. E. (2000). “2-D and 3-D Numerical Simulation of Abrupt Transitions in Open-Channel Flows. Application to the Design of Canoe Chutes.” *Proc. 4th International Conference on Hydroinformatics, International Association for Hydraulic Resesarch*, Iowa City, IA, July 23-27.

[7] Bradford, S. F., and Katopodes, N. D. (1999a). "Hydrodynamics of turbid underflows. I: formulation and numerical analysis.” *J. Hyd. Eng.*, ASCE, 125(10), 1006-1015.

[8] Bradford, S. F., and Katopodes, N. D. (1999b). "Hydrodynamics of turbid underflows. II: agradation, avulsion, and channelization.” *J. Hyd. Eng.*, ASCE, 125(10), 1016-1028.

[9] Caisley, M. E., Bombardelli, F. A., and García, M. H. (1999). “Physical and numerical Studies of Canoe Chutes for Low-Head Dams in Illinois.” *Proc. World FLOW-3D® User’s Conf.*, Santa Fe, New Mexico, September 27-28.

[10] Choi, S.-U. (1996). “Layer-averaged modeling of turbidity currents with a finite element method.” Ph. D. Thesis, University of Illinois at Urbana-Champaign.

[11] Choi, S.-U., and García, M. H. (1995). “Modeling of one-dimensional turbidity currents with a dissipative-Galerkin finite element method.” *J. Hyd. Research*, 33(5), 623-648.

[12] Chrzastowski, M. J. (1998). “Geology of the Chicago Lakeshore. The Chicago River mouth”, poster prepared by the Illinois State Geological Survey.

[13] Crook, N. A. and Miller, M. J. (1985). “A numerical and analytical study of atmospheric undular bores.” *Quart. J. R. Met. Soc.*, 111, 225-242.

[14] Daly, B. J., and Pratch, W. E. (1968). “Numerical study of density current surges.” *Phys. Fluids* 11, 15-30.

[15] FLOW-3D® User’s Manual (2000). *Flow Science, Inc. Report 00-00-01; www.flow3d.com*.

[16] Ford, D. E., and Johnson, M. C. (1983). “An assessment of reservoir mixing processes.” *Technical Report Nº E-83-7, U.S. Army Engineer Waterways Experiment Station*, Vicksburg, MS.

[17] García, M. H. (1990). "Depositing and eroding sediment-driven flows: turbidity currents." *Proj. Rep. No. 306*, St. Anthony Falls Hydraulic Lab., Univ. of Minnesota, Minneapolis, Minn., 179.

[18] García, M. H. (1992). "Turbidity currents." *Encyclopedia of earth systems science*, 4, Academic Press, San Diego, Calif., 399-408.

[19] García, M. H. (1994). "Depositional turbidity currents laden with poorly sorted sediment." *J. Hyd. Eng.*, ASCE, 120(11), 1240-1263.

[20] Gill, A. E. (1982). “Appendix 3, Properties of Seawater.” *Atmosphere-Ocean Dynamics*, Academic Press, New York, 599-600.

[21] Haase, S. P., and Smith, R. K. (1989). “The numerical simulation of atmospheric gravity currents. Part II. Environments with stable layers.” *Geophys. Astrophys. Fluid Dynamics*, 46, 35-51.

[22] Lanyon, R. (2000). “Chicago river reversal solves public health crisis.” *Wetland matters*, 5(2).

[23] Lin, P. C.-P., and Mehta, A. J. (1996). “A study of fine sedimentation in an elongated laboratory basin.” *J. Coastal Research*, Special Issue, Royal Palm Beach, 25, 19-30.

[24] Mitchell, K. E., and Hovermale, J. B. (1977). “A numerical investigation of the severe thunderstorm gust front.” *Monthly weather review*, 105, 657-675.

[25] Polls, I., Sawyer, B., Tata, P., and Lanyon, R. (2000). “Water quality in the North and South Branches of the Chicago River, and inshore area of Lake Michigan during November and December 1999.” Report of the Metropolitan Water Reclamation District of Greater Chicago, Chicago.

[26] Rodríguez, J. F., Bombardelli, F. A., García, M. H., Guzmán, J. M., Frothingham, K. and Rhoads, B. L. (2000). “Numerical modeling of meandering streams.” *Proc. 4th International Conference on Hydroinformatics, International Association for Hydraulic Resesarch*, Iowa City, IA, July 23-27.

[27] Snoeyink, V. L., and Jenkins, D. (1987). “Water chemistry.” Editorial Limusa, México (in Spanish).

[28] Straka, J. M., Wilhelmson, R. B., Wicker, L. J., Anderson, J. R., and Droegemeier, K. K. (1993). “Numerical solutions of a non-linear density current: a benchmark solution and comparisons.” *Int. J. Num. Meth, Fluids*, 17, 1-22.

[29] Thorpe, A. J., Miller, M. J., and Moncrieff, M. W. (1980). “Dynamical models of two-dimensional downdraughts.” *Quart. J. R. Met. Soc.*, 106, 463-484.

[30] United States Geological Survey (2000). “Specific electrical conductance”, TWRI Book 9, Water Resources, Office of Water Quality, http://water.usgs.gov.

[31] Wüest, A., Brooks, N. H., and Imboden, D. M. (1992). “Bubble plume modeling for lake restoration.” *Water Resources Res.*, 28(12), 3235-3250.

# APPENDIX 1

# SUMMARY OF DATA COLLECTED BY USGS

## SUMMARY OF DATA COLLECTED BY USGS

| | | 20 | | 40 | | 60 | | 80 | | 100 | |
|---|---|---|---|---|---|---|---|---|---|---|---|
| Distance from surface | | 6.1 | | 12.19 | | 18.29 | | 24.38 | | 30.48 | |
| feet | m | T (C) | SC (*u* S/cm) | T (C) | SC (*u* S/cm) | T (C) | SC (*u* S/cm) | T (C) | SC (*u* S/cm) | T (C) | SC (*u* S/cm) |
| 0 | 0 | 3.06 | 607 | 2.87 | 606 | 2.82 | 613 | 2.8 | 609 | 2.79 | 611 |
| 2 | 0.61 | 3 | 607 | 2.84 | 612 | 2.8 | 608 | 2.78 | 610 | 2.78 | 610 |
| 4 | 1.22 | 2.98 | 608 | 2.81 | 618 | 2.78 | 617 | 2.75 | 623 | 2.8 | 617 |
| 6 | 1.83 | 2.99 | 616 | 2.85 | 627 | 2.79 | 622 | 2.74 | 625 | 2.77 | 626 |
| 8 | 2.44 | 3 | 616 | 2.89 | 673 | 2.81 | 656 | 2.79 | 659 | 2.77 | 650 |
| 10 | 3.05 | 3 | 642 | 2.95 | 716 | 2.88 | 698 | 2.88 | 703 | 2.88 | 700 |
| 12 | 3.66 | 3.11 | 715 | 3 | 742 | 2.96 | 729 | 2.94 | 732 | 2.95 | 733 |
| 14 | 4.27 | 3.13 | 737 | 3.04 | 757 | 3 | 753 | 2.96 | 743 | 2.96 | 740 |
| 16 | 4.88 | 3.14 | 746 | 3.14 | 808 | 3.03 | 770 | 2.98 | 754 | 2.97 | 752 |
| 18 | 5.49 | 3.15 | 755 | 3.41 | 318 | 3.15 | 828 | 3 | 767 | 2.99 | 763 |
| 20 | 6.1 | 3.26 | 824 | 3.73 | 1020 | 3.67 | 967 | 3.09 | 798 | 3.04 | 809 |
| 22 | 6.71 | 3.45 | 888 | 3.88 | 1080 | 3.87 | 1073 | 3.43 | 891 | 3.23 | 868 |
| 24 | 7.32 | 3.64 | 998 | 3.96 | 1100 | 3.96 | 1118 | 3.6 | 963 | 3.55 | 965 |
| 26 | 7.92 | 4.01 | 1083 | | | 3.99 | 1120 | 3.79 | 1063 | 3.68 | 1085 |
| 28 | 8.53 | | | | | | | 3.88 | 1079 | 3.91 | 1122 |
| 30 | 9.14 | | | | | | | 3.87 | 1097 | | |
| 32 | 9.75 | | | | | | | 3.92 | 1111 | | |

| | | 120 | | 140 | | 160 | | 180 | | 220 | |
|---|---|---|---|---|---|---|---|---|---|---|---|
| Distance from surface | | 36.58 | | 42.67 | | 48.77 | | 54.86 | | 67.06 | |
| feet | m | T (C) | SC (*u* S/cm) | T (C) | SC (*u* S/cm) | T (C) | SC (*u* S/cm) | T (C) | SC (*u* S/cm) | T (C) | SC (*u* S/cm) |
| 0 | 0 | 2.79 | 611 | 2.8 | 612 | 2.81 | 611 | 2.82 | 611 | 2.82 | 611 |
| 2 | 0.61 | 2.79 | 611 | 2.8 | 612 | 2.8 | 611 | 2.81 | 611 | 2.82 | 612 |
| 4 | 1.22 | 2.78 | 620 | 2.8 | 626 | 2.8 | 612 | 2.8 | 609 | 2.8 | 617 |
| 6 | 1.83 | 2.75 | 632 | 2.78 | 635 | 2.8 | 620 | 2.8 | 669 | 2.85 | 697 |
| 8 | 2.44 | 2.78 | 660 | 2.82 | 670 | 2.8 | 641 | 2.9 | 732 | 2.94 | 740 |
| 10 | 3.05 | 2.87 | 700 | 2.91 | 714 | 2.88 | 696 | 2.95 | 754 | 2.96 | 744 |
| 12 | 3.66 | 2.94 | 730 | 2.96 | 738 | 2.96 | 742 | 3.04 | 795 | 2.97 | 756 |
| 14 | 4.27 | 2.96 | 754 | 2.97 | 753 | 2.97 | 752 | 3.24 | 861 | 3.05 | 796 |
| 16 | 4.88 | 3 | 762 | 3.01 | 782 | 3.1 | 801 | | | 3.25 | 861 |
| 18 | 5.49 | 3.07 | 811 | 3.12 | 880 | 3.14 | 850 | | | 3.64 | 976 |
| 20 | 6.1 | 3.36 | 894 | 3.73 | 1004 | | | | | | |
| 22 | 6.71 | 3.5 | 946 | | | | | | | | |
| 24 | 7.32 | 3.88 | 1110 | | | | | | | | |
| 26 | 7.92 | | | | | | | | | | |
| 28 | 8.53 | | | | | | | | | | |
| 30 | 9.14 | | | | | | | | | | |
| 32 | 9.75 | | | | | | | | | | |

**Table 2.1a:** Temperature and specific conductance measurements at Lake Shore Drive (03/19/98)

| | | Distance from water edge. (feet) (m) | | | | | | | | | | | |
|---|---|---|---|---|---|---|---|---|---|---|---|---|---|
| | | 10 | | 50 | | 90 | | 130 | | 170 | | 190 | |
| Distance from surface | | 3.05 | | 15.24 | | 27.43 | | 39.62 | | 51.82 | | 57.91 | |
| feet | m | T (C) | SC (*u*S/cm) | T (C) | SC (*u*S/cm) | T (C) | SC (*u*S/cm) | T (C) | SC (*u*S/cm) | T (C) | SC (*u*S/cm) | T (C) | SC (*u*S/cm) |
| 0 | 0.00 | 2.97 | 659 | 2.92 | 660 | 2.94 | 660 | 2.95 | 654 | 2.97 | 660 | 2.98 | 665 |
| 2 | 0.61 | 2.96 | 660 | 2.92 | 659 | 2.93 | 660 | 2.91 | 664 | 2.94 | 665 | 2.96 | 665 |
| 4 | 1.22 | 2.96 | 660 | 2.92 | 660 | 2.92 | 660 | 2.87 | 676 | 2.87 | 675 | 2.96 | 679 |
| 6 | 1.83 | 2.94 | 659 | 2.92 | 660 | 2.89 | 693 | 2.89 | 698 | 2.91 | 706 | 2.91 | 681 |
| 8 | 2.44 | 2.94 | 660 | 2.94 | 710 | 2.96 | 741 | 2.91 | 716 | 2.95 | 726 | 2.93 | 705 |
| 10 | 3.05 | 2.96 | 681 | 3.00 | 751 | 3.15 | 808 | 3.12 | 774 | 3.30 | 820 | 2.94 | 719 |
| 12 | 3.66 | 3.05 | 747 | 3.09 | 794 | 3.31 | 848 | 3.31 | 835 | 3.46 | 853 | 3.28 | 803 |
| 14 | 4.27 | 3.19 | 800 | 3.28 | 838 | 3.52 | 955 | 3.42 | 889 | 3.56 | 938 | 3.54 | 862 |
| 16 | 4.88 | 3.22 | 822 | 3.45 | 919 | 3.90 | 1068 | 3.70 | 1015 | 3.89 | 1062 | 3.52 | 880 |
| 18 | 5.49 | 3.41 | 885 | 3.70 | 1038 | 4.21 | 1156 | 4.00 | 1084 | 3.96 | 1082 | | |
| 20 | 6.10 | 3.55 | 947 | 3.77 | 1090 | | | 4.15 | 1142 | | | | |
| 22 | 6.71 | 3.70 | 1045 | | | | | | | | | | |
| 24 | 7.32 | 4.13 | 1150 | | | | | | | | | | |

**Table 2.1b:** Temperature and specific conductance measurements at Columbus Drive (03/19/98)

| | | Distance from water edge. (feet) (m) | | | | | | | | | | | |
|---|---|---|---|---|---|---|---|---|---|---|---|---|---|
| | | 0 | | 50 | | 90 | | 130 | | 170 | | 200 | |
| Distance from surface | | 0 | | 15.24 | | 27.43 | | 39.62 | | 51.82 | | 60.96 | |
| feet | m | T (C) | SC (*u*S/cm) | T (C) | SC (*u*S/cm) | T (C) | SC (*u*S/cm) | T (C) | SC (*u*S/cm) | T (C) | SC (*u*S/cm) | T (C) | SC (*u*S/cm) |
| 0 | 0.00 | 2.99 | 680 | 2.96 | 681 | 2.99 | 692 | 3.02 | 700 | 3.09 | 700 | 3.22 | 702 |
| 2 | 0.61 | 2.99 | 680 | 2.97 | 679 | 2.98 | 680 | 3.01 | 706 | 3.05 | 705 | 3.21 | 703 |
| 4 | 1.22 | 3.01 | 692 | 2.97 | 677 | 2.99 | 684 | 3.01 | 707 | 3.04 | 709 | 3.15 | 706 |
| 6 | 1.83 | 3.05 | 709 | 2.97 | 679 | 3.01 | 695 | 3.02 | 704 | 3.04 | 707 | 3.13 | 708 |
| 8 | 2.44 | 3.10 | 735 | 2.98 | 685 | 3.07 | 717 | 3.03 | 713 | 3.03 | 713 | 3.38 | 711 |
| 10 | 3.05 | 3.16 | 759 | 3.26 | 806 | 3.12 | 743 | 3.12 | 741 | 3.03 | 728 | 3.39 | 713 |
| 12 | 3.66 | 3.23 | 796 | 3.32 | 831 | 3.37 | 783 | 3.48 | 812 | 3.18 | 738 | 3.46 | 775 |
| 14 | 4.27 | 3.39 | 865 | 3.34 | 838 | 3.46 | 810 | 3.40 | 863 | 3.48 | 861 | 3.52 | 886 |
| 16 | 4.88 | | | 3.34 | 848 | 3.41 | 860 | 3.67 | 982 | 3.76 | 1001 | 3.57 | 925 |
| 18 | 5.49 | | | 3.79 | 981 | 3.57 | 943 | 4.02 | 1081 | | | | |
| 20 | 6.10 | | | 4.01 | 1050 | 4.13 | 1050 | 4.06 | 1115 | | | | |
| 22 | 6.71 | | | 4.06 | 1086 | 4.07 | 1130 | | | | | | |
| 24 | 7.32 | | | 4.17 | 1149 | | | | | | | | |

**Table 2.1c:** Temperature and specific conductance measurements at Michigan Avenue (03/19/98)

| | | Distance from water edge. (f) (m) | | | | | | | | | | | |
|---|---|---|---|---|---|---|---|---|---|---|---|---|---|
| | | 20 | | 60 | | 100 | | 140 | | 180 | | 210 | |
| Distance from surface | | 6.10 | | 18.29 | | 30.48 | | 42.67 | | 54.86 | | 64.01 | |
| feet | m | T (C) | SC (*u*S/cm) | T (C) | SC (*u*S/cm) | T (C) | SC (*u*S/cm) | T (C) | SC (*u*S/cm) | T (C) | SC (*u*S/cm) | T (C) | SC (*u*S/cm) |
| 0 | 0.00 | 3.04 | 707 | 3.08 | 704 | 3.02 | 708 | 3.05 | 715 | 3.09 | 718 | 3.12 | 723 |
| 2 | 0.61 | 3.03 | 709 | 3.03 | 705 | 3.03 | 708 | 3.06 | 716 | 3.09 | 720 | 3.13 | 727 |
| 4 | 1.22 | 3.11 | 752 | 3.09 | 736 | 3.06 | 730 | 3.09 | 744 | 3.09 | 729 | 3.15 | 729 |
| 6 | 1.83 | 3.22 | 790 | 3.16 | 785 | 3.10 | 755 | 3.21 | 777 | 3.10 | 743 | 3.20 | 761 |
| 8 | 2.44 | 3.27 | 802 | 3.21 | 808 | 3.15 | 772 | 3.34 | 841 | 3.22 | 785 | 3.24 | 781 |
| 10 | 3.05 | 3.34 | 828 | 3.24 | 814 | 3.29 | 800 | 3.61 | 904 | 3.50 | 883 | 3.41 | 845 |
| 12 | 3.66 | 3.38 | 840 | 3.34 | 832 | 3.37 | 832 | 4.05 | 1023 | 3.41 | 867 | | |
| 14 | 4.27 | 3.39 | 847 | 3.62 | 928 | 3.41 | 846 | 4.04 | 1020 | | | | |
| 16 | 4.88 | 3.43 | 863 | 4.10 | 1036 | 3.57 | 896 | 4.12 | 1060 | | | | |
| 18 | 5.49 | 3.68 | 972 | 4.23 | 1085 | 4.08 | 1006 | | | | | | |
| 20 | 6.10 | | | | | 4.13 | 1060 | | | | | | |
| 22 | 6.71 | | | | | 4.27 | 1144 | | | | | | |

**Table 2.1d:** Temperature and specific conductance measurements at Wabash Avenue (03/19/98)

| | | Distance from water edge. (f) (m) | | | | | | | | | |
|---|---|---|---|---|---|---|---|---|---|---|---|
| | | 20 | | 60 | | 100 | | 140 | | 180 | |
| Distance from surface | | 6.10 | | 18.29 | | 30.48 | | 42.67 | | 54.86 | |
| feet | m | T (C) | SC (*u*S/cm) | T (C) | C (*u*S/cm) | T (C) | SC (*u*S/cm) | T (C) | SC (*u*S/cm) | T (C) | SC (*u*S/cm) |
| 0 | 0.00 | 3.81 | 732 | 3.95 | 724 | 3.07 | 719 | 3.06 | 711 | 3.19 | 726 |
| 2 | 0.61 | 3.24 | 731 | 3.37 | 724 | 3.07 | 723 | 3.07 | 712 | 3.18 | 727 |
| 4 | 1.22 | 3.21 | 734 | 3.12 | 725 | 3.09 | 736 | 3.07 | 723 | 3.17 | 726 |
| 6 | 1.83 | 3.19 | 771 | 3.11 | 726 | 3.09 | 733 | 3.10 | 725 | 3.15 | 726 |
| 8 | 2.44 | 3.19 | 780 | 3.12 | 747 | 3.09 | 736 | 3.09 | 726 | 3.13 | 727 |
| 10 | 3.05 | 3.19 | 785 | 3.12 | 755 | 3.10 | 737 | 3.33 | 801 | 3.43 | 808 |
| 12 | 3.66 | 3.14 | 829 | 3.17 | 772 | 3.28 | 793 | 4.48 | 1050 | 3.75 | 896 |
| 14 | 4.27 | 3.64 | 919 | 3.26 | 806 | 4.02 | 981 | | | 4.20 | 1010 |
| 16 | 4.88 | | | 3.67 | 940 | 4.29 | 1050 | | | 4.54 | 1081 |
| 18 | 5.49 | | | 4.15 | 1062 | 4.32 | 1115 | | | 4.58 | 1051 |
| 20 | 6.10 | | | 4.43 | 1174 | | | | | | |

**Table 2.1e:** Temperature and specific conductance measurements at State Street (03/19/98)

| | | Distance from water edge. (feet) (m) | | | | | | | | | |
|---|---|---|---|---|---|---|---|---|---|---|---|
| | | 20 | | 60 | | 100 | | 140 | | 180 | |
| Distance from surface | | 6.10 | | 18.29 | | 30.48 | | 42.67 | | 54.86 | |
| Feet | m | T (C) | SC (*u*S/cm) | T (C) | C (*u*S/cm) | T (C) | SC (*u*S/cm) | T (C) | SC (*u*S/cm) | T (C) | SC (*u*S/cm) |
| 0 | 0.00 | 3.51 | 824 | 3.57 | 832 | 3.64 | 837 | 3.70 | 854 | 3.88 | 870 |
| 2 | 0.61 | 3.53 | 831 | 3.57 | 832 | 3.64 | 841 | 3.74 | 852 | 3.97 | 879 |
| 4 | 1.22 | 3.57 | 840 | 3.96 | 860 | 3.66 | 845 | 4.12 | 892 | 4.02 | 884 |
| 6 | 1.83 | 3.67 | 846 | 4.21 | 894 | 4.20 | 878 | 4.29 | 910 | 4.58 | 917 |
| 8 | 2.44 | 3.96 | 879 | 4.23 | 913 | 4.47 | 915 | 4.80 | 942 | 4.71 | 944 |
| 10 | 3.05 | 4.39 | 944 | 4.86 | 952 | 4.67 | 940 | 4.98 | 962 | 4.69 | 943 |
| 12 | 3.66 | 4.88 | 975 | 4.96 | 970 | 4.84 | 953 | 5.16 | 973 | 4.62 | 940 |
| 14 | 4.27 | 4.97 | 984 | 5.04 | 974 | 5.01 | 965 | 5.20 | 984 | 5.27 | 975 |
| 16 | 4.88 | 5.13 | 1007 | 5.15 | 991 | 5.19 | 996 | 5.20 | 995 | 5.44 | 992 |
| 18 | 5.49 | 5.28 | 1006 | 5.34 | 1016 | 5.24 | 1011 | 5.25 | 1010 | | |

**Table 2.1f:** Temperature and specific conductance measurements at State Street (03/19/98)

| | | Distance from water edge y (f) and (m) | | | | | | | | | |
|---|---|---|---|---|---|---|---|---|---|---|---|
| | | 0 | 20 | 40 | 60 | 80 | 100 | 120 | 140 | 160 | 184 |
| Distance from surface | | 0.00 | 6.10 | 12.19 | 18.29 | 24.38 | 30.48 | 36.58 | 42.67 | 48.77 | 56.08 |
| feet | m | T (C) | T (C) | T (C) | T (C) | T (C) | T (C) | T (C) | T (C) | T (C) | T (C) |
| 0 | 0.00 | 5.50 | 5.50 | 5.60 | 5.60 | 5.60 | 5.60 | 5.70 | 5.80 | 5.80 | 5.70 |
| 2 | 0.61 | 5.50 | 5.50 | 5.60 | 5.60 | 5.60 | 5.60 | 5.70 | 5.70 | 5.80 | 5.70 |
| 4 | 1.22 | 5.40 | 5.50 | 5.60 | 5.60 | 5.60 | 5.60 | 5.60 | 5.70 | 5.80 | 5.70 |
| 6 | 1.83 | 5.50 | 5.50 | 5.60 | 5.60 | 5.60 | 5.60 | 5.60 | 5.70 | 5.70 | 5.70 |
| 8 | 2.44 | 5.50 | 5.50 | 5.60 | 5.60 | 5.60 | 5.60 | 5.60 | 5.70 | 5.50 | 5.70 |
| 10 | 3.05 | 5.50 | 5.50 | 5.60 | 5.60 | 5.60 | 5.60 | 5.60 | 5.70 | 5.60 | 5.60 |
| 12 | 3.66 | 5.50 | 5.50 | 5.60 | 5.60 | 5.60 | 5.60 | 5.60 | 5.70 | 5.50 | 5.50 |
| 14 | 4.27 | 5.50 | 5.50 | 5.60 | 5.80 | 5.60 | 5.60 | 5.60 | 5.70 | 5.50 | 5.60 |
| 16 | 4.88 | 6.60 | 7.10 | 5.60 | 5.80 | 6.50 | 7.40 | 7.10 | 6.80 | 6.10 | 6.50 |
| 18 | 5.49 | 6.95 | 7.30 | 7.20 | 7.10 | 7.40 | 7.40 | 7.40 | 7.40 | 6.70 | 6.90 |
| 20 | 6.10 | 6.97 | 7.35 | 7.40 | 7.40 | 7.40 | 7.40 | 7.40 | 7.40 | 7.30 | 7.30 |
| 22 | 6.71 | | | | | 7.40 | 7.40 | 7.40 | | 7.30 | 7.30 |

**Table 2.1g:** Temperature measurements at Columbus Drive (02/24/98)

# APPENDIX 2

# APPENDIX 2
# FLOW-3D® COMPUTATIONAL MODEL

## A2.1 GENERAL CONCEPTS

FLOW-3D® is a powerful 3-D numerical code developed by Flow Science, Inc., Los Alamos, USA, for Computational Fluid Dynamics (CFD) problems. Former Los Alamos National Laboratory researchers, who proposed several leading techniques in CFD at that institution, founded Flow Science, Inc. Those leading techniques are now part of the code.

The solver allows for the solution of very complex problems, for laminar or turbulent, compressible or incompressible flows. To accomplish that, FLOW-3D® solves the fully-3-D transient Navier-Stokes equations by a finite-volume-finite-difference method in a fixed (Eulerian) rectangular grid. It includes a variety of processes that are interesting to simulate water flows, such as heat conduction, surface tension, cavitation and moving obstacles. For turbulent flows, it supports closure through a number of advanced and widely accepted approximations, including:

a) Prandtl's mixing length theory;
b) turbulent energy model;
c) two-equation $k-\varepsilon$ model and
d) $k-\varepsilon$ RNG, based on the Renormalization Group Theory,

solved together with the Reynolds-Averaged Navier-Stokes (RANS) equations. A version of the filtered Navier-Stokes equations is also implemented (Flow Science, 2000).

In FLOW-3D®, the processes of meshing and building the obstacles in the model are totally independent. This property avoids the laborious tasks related to the construction of body-fitted meshes (to conform to obstacle shapes) or to the creation of finite-element grids. On the opposite point of view, this procedure needs densification when the domain is very sinuous. In turn, the obstacles and the full geometry are defined independently from the mesh by a "solid modeler", which allows for the use of general quadratic functions, or through Computer Aided Design (CAD). In order to represent the solid boundaries, the FAVOR technique is employed (Hirt and Sicilian, 1985), which incorporates fractions of volumes and areas to account for the parts of the finite volume open to flow in the computation of the fluxes. In this way, some volumes may be blocked whereas some others are partially or totally open. Thus, FAVOR precludes saw-tooth representations of solid boundaries.

The meshing process produces a smooth variation of the cell size in order to maintain numerical accuracy. A staggered grid for the velocities is utilized. The numerical scheme has an accuracy that is in general first order with respect to time and space increments. The numerical implementation of the numerical scheme is explicit.

Second order discretization of the advective and viscous terms is also available.

## A2.2 VOF FREE-SURFACE COMPUTATION METHOD

Several methods have been devised in order to treat the free surface. The free surface is not only unknown but also acts as a boundary condition for the problem. Therefore, this fact adds more complexity to the well-known difficulty of 3-D numerical simulations.

A detailed follow-up of the free surface is complex to code and it gets almost impracticable for cases in which volumes of water break apart. Three problems arise: how to compute it, the amount of computation time needed and the minimum number of

variables to be stored in the process. As a consequence, alternative solutions for special cases have been proposed.

The most frequently found technique in hydraulics is the “rigid lid” approximation, which assumes the free surface as a horizontal plane. The pressure field calculated by the model gives in this approximation the displacements of the free surface with respect to that plane. Other methods are based on the use of ad-hoc cells of different size located close to the water surface, and some authors have employed a “porosity” technique. A variable density that is equal to the water’s value in the aqueous phase and zero outside has been also implemented in several codes.

FLOW-3D® uses the Volume-of-Fluid (VOF) method (Hirt and Nichols, 1981), which is based on defining a function ($F$, the volume fraction) whose value is one at any point occupied by fluid and zero everywhere else. Between these two extreme values, a complete set of values can be found. In conjunction with a numerical model, the average value of this function over each grid element is equal to the fractional volume of the element occupied by fluid. At each time step, the following equation for the above function is solved:

$$\frac{\partial F}{\partial t} + u_i \frac{\partial F}{\partial x_i} = 0 \qquad \text{(A2.1)}$$

where $u_i$ is the i-th component of the velocity vector, $x_i$ indicates the spatial coordinates and $t$ refers to the time coordinate. The method is based on three key elements: the definition of the function $F$, the use of a high-accuracy numerical scheme to solve A2.1 avoiding numerical diffusion and the specification of appropriate boundary conditions at the free surface, consisting in the setting of null tangential stresses. This method combines the advantages of minimum memory storage (only one variable, $F$, has to be recorded), reasonable computational cost and satisfactory accuracy.

## A2.3 BOUNDARY CONDITIONS

FLOW-3D® can handle a variety of boundary conditions, as follows:

a) rigid wall with slip;
b) rigid wall with no-slip (imposed through a wall shear stress);
c) specification of fixed velocities or pressures;
d) symmetry planes;
e) continuative outflow boundaries;
f) periodic boundaries.

The boundary conditions for the turbulent kinetic energy and the dissipation rate are the usual ones. For rigid walls, wall functions are used to compute the values for the variables in the first control volume close to the boundary; null derivatives of those variables normal to the boundaries are set in the case of symmetry planes. When dealing with free surfaces, the physical behavior of the boundary has some properties similar to a rigid wall (the fluctuations vanish perpendicularly to the surface) and some other properties resemble a symmetry plane; therefore, it could be treated either way. In FLOW-3D®, the free surface is treated as a symmetry plane.

These boundary conditions differ from other models' conditions, in the FAVOR technique included in FLOW-3D®.

## A2.4 SIMULATION OF STRATIFIED FLOWS WITH FLOW-3D®

FLOW-3D® allows for the simulation of stratified flows in the following ways:

a) *As a single fluid with variable density*;
b) *As a two-fluid flow*.

In particular, single-fluid variable-density flows can be treated together with a volume tracking of the free surface or with the *drift-model approximation*. The first type of model applies to flows in which density varies spatially in an otherwise incompressible flow. The latter refers to a simple two-phase flow in which one component of a mixture can move with respect to another; it is a good model if the relative velocity between the fluids is quite small and it is not suitable for free-surface tracking. This last approximation proved to be satisfactory for the simulation of laboratory generated density currents (García and Bombardelli, unpublished report).

In the simulations reported herein, the flow was treated as a single-fluid variable-density flow.

## REFERENCES


[A2.1] FLOW-3D® User's Manual (2000). *Flow Science, Inc. Report 00-01-01; www.flow3d.com*.

[A2.2] Hirt, C. W., and Nichols, B. D. (1981). "Volume of Fluid (VOF) method for the dynamics of free boundaries." *J. Comp. Phys.*, 39, 201-225.

[A2.3] Hirt, C. W., and Sicilian, J. M. (1985). "A porosity technique for the definition of obstacles in rectangular cell meshes." *Proc. Fourth Int. Conf. Ship Hydro.,* National Academy of Science, Washington, DC.

# APPENDIX 3

# APPENDIX 3
# NUMERICAL SIMULATION OF LIN-MEHTA TESTS

## A3.1 OBJECTIVE OF THE SIMULATIONS. LIN-MEHTA TESTS

The objective of this numerical exercise was to analyze the performance of the selected theoretical model to simulate density currents.

P. C.-P. Lin and A. J. Mehta presented in 1997 a study about sedimentation in elongated basins. In estuarine environments, turbidity currents play an important rôle transporting suspended sediment to neighboring basins; if the advective transport is limited, these small basins are prone to sedimentation by this mechanism. To study this phenomenon, Lin and Mehta performed measurements in a laboratory basin 14 m long, 0.1 m wide with a depth of 0.1 m. The device is as follows:

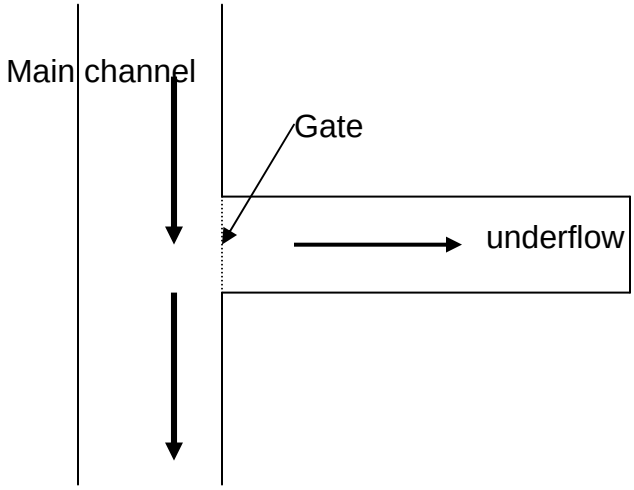


**Figure A3.1:** Schematization of the tests

Initially, Lin and Mehta generated a sediment-laden (denser) water current in the main channel and introduced lighter water in the basin, separating both fluids through a gate. They later released the gate and measured the front position for different times.

The measurements were performed for diverse density differences and diverse settling velocities (different particle sediment size). They considered that the width of the basin does not play a significant rôle in the determination of the features of the density current. Figure A3.2 presents their results in terms of the evolution of the front position in time. In the expression for the normalized time, they employed the densimetric velocity or interfacial celerity, as follows:

$$u_{\Delta} = \sqrt{g \frac{\Delta\rho}{\rho_w} H} \qquad \text{(A3.1)}$$

*Among their very interesting results, Lin and Mehta identified that the behavior of the turbidity current, carrying sediment, was similar to that pertaining to a viscous non-turbulent flow, i.e., that the behavior was mainly viscous. They have also found that turbid fronts (with sediment) behave similarly to non-settling gravity fronts*.

The above experiments were implemented in FLOW-3D® to facilitate the comparison. The solid modeler was used to set the geometry. The conditions corresponding to Test Nº 1 were taken, for which: $\Delta\rho$ = 1.04 kg/m$^3$, $w_{s1}$ (settling velocity) = 0.048 10$^{-2}$ m/s and $u_{\Delta}$ = 0.032 m/s. Figure A3.2 presents the comparison between the measured and modeled front position vs time. A satisfactory agreement can be noticed between them.

Finally, notice that the conditions studied by Lin and Mehta, and modeled with FLOW-3D®, resemble those at the CR.

**REFERENCES**

[A3.1] FLOW-3D® User's Manual (2000). *Flow Science, Inc. Report 00-01-01; www.flow3d.com*.

[A3.2] Lin, P. C.-P., and Mehta, A. J. (1996). “A study of fine sedimentation in an elongated laboratory basin.” *J. Coastal Research*, Special Issue, Royal Palm Beach, 25, 19-30.

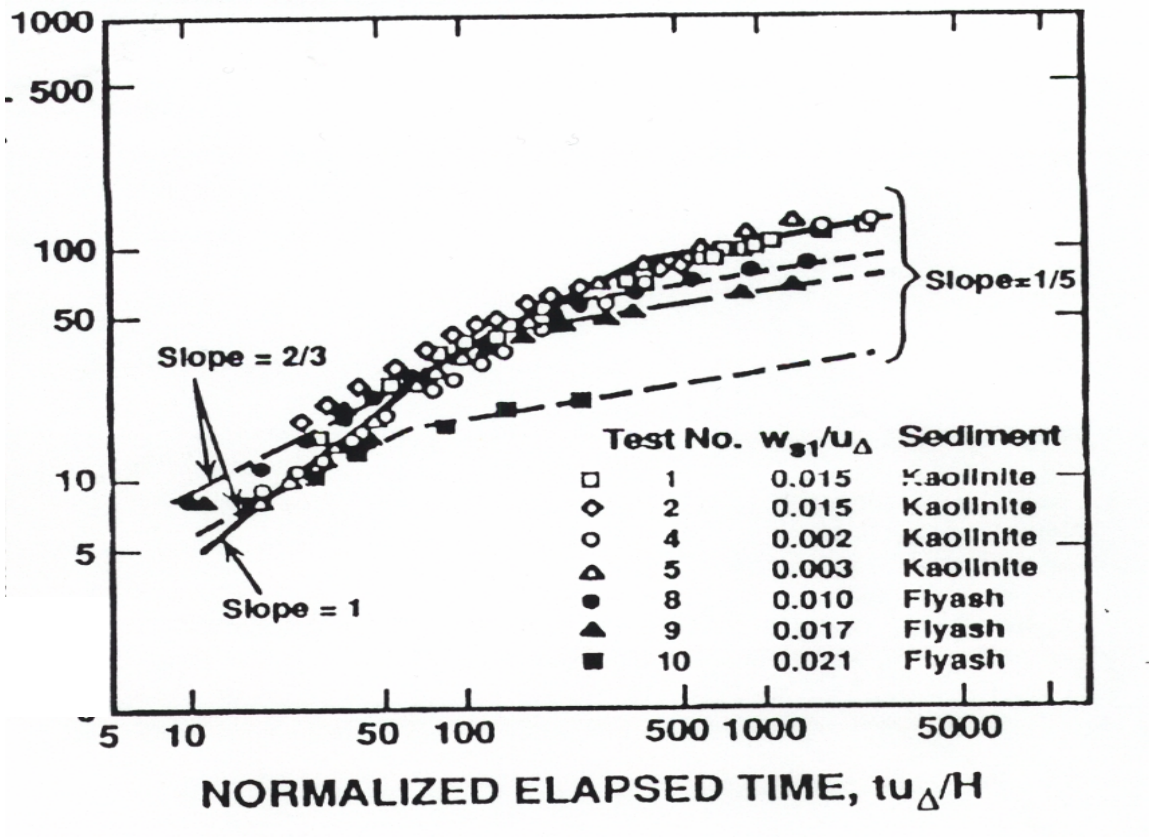


**Figure A3.2:** Tests by Lin and Mehta

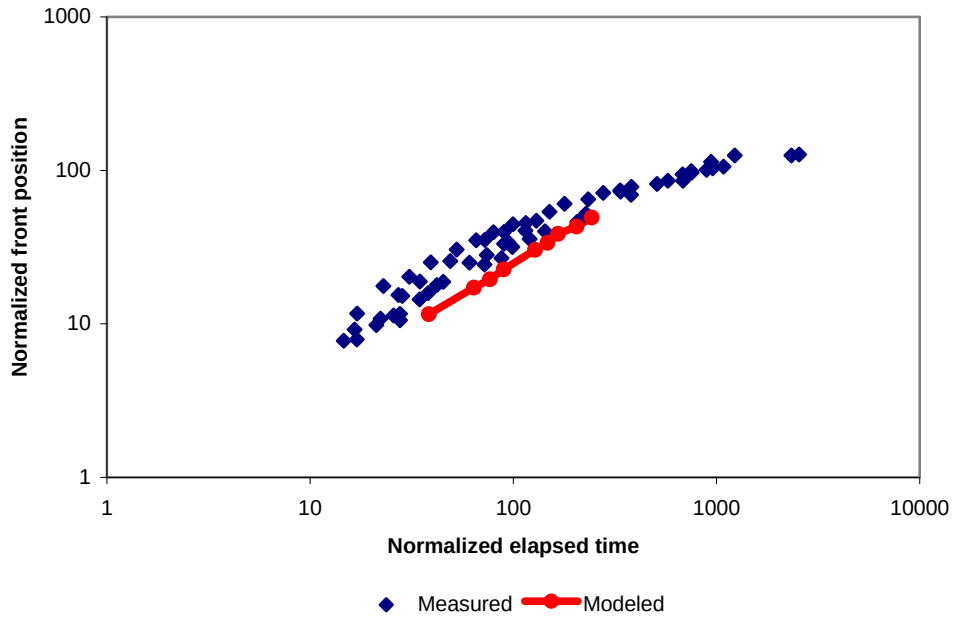


**Figure A3.3:** Comparison between measured and modeled values for Lin and Mehta's tests